J. metamorphic Geol., 2004, **22,** 207–226 doi:10.1111/j.1525-1314.2004.00509.x

Late Miocene movement within the Himalayan Main Central Thrust shear zone, Sikkim, north-east India

E. J. CATLOS,[1] C. S. DUBEY,[2] T. M. HARRISON[3] AND M. A. EDWARDS[4]
[1]*School of Geology, Oklahoma State University, Stillwater, Oklahoma, OK 74078, USA (catlos@okstate.edu)*
[2]*Department of Geology, University of Delhi, India*
[3]*Research School of Earth Sciences, The Australian National University Canberra, ACT 0200, Australia*
[4]*Structural Processes Group, Institut für Geologie, University of Vienna, Althanstrasse 14, Vienna A-1090, Austria*

ABSTRACT In the Sikkim region of north-east India, the Main Central Thrust (MCT) juxtaposes high-grade gneisses of the Greater Himalayan Crystallines over lower-grade slates, phyllites and schists of the Lesser Himalaya Formation. Inverted metamorphism characterizes rocks that immediately underlie the thrust, and the large-scale South Tibet Detachment System (STDS) bounds the northern side of the Greater Himalayan Crystallines. *In situ* Th–Pb monazite ages indicate that the MCT shear zone in the Sikkim region was active at *c.* 22, 14–15 and 12–10 Ma, whereas zircon and monazite ages from a slightly deformed horizon of a High Himalayan leucogranite within the STDS suggest normal slip activity at *c.* 17 and 14–15 Ma. Although average monazite ages decrease towards structurally lower levels of the MCT shear zone, individual results do not follow a progressive younging pattern. Lesser Himalaya sample KBP1062A records monazite crystallization from 11.5 ± 0.2 to 12.2 ± 0.1 Ma and peak conditions of 610 ± 25 °C and 7.5 ± 0.5 kbar, whereas, in the MCT shear zone rock CHG14103, monazite crystallized from 13.8 ± 0.5 to 11.9 ± 0.3 Ma at lower grade conditions of 525 ± 25 °C and 6 ± 1 kbar. The *P–T–t* results indicate that the shear zone experienced a complicated slip history, and have implications for the understanding of mid-crustal extrusion and the role of out-of-sequence thrusts in convergent plate tectonic settings.

Key words: geochronology; Main Central Thrust; monazite; Sikkim Himalayas; thermobarometry.

INTRODUCTION

The Himalayan mountains were created by the collision of India with Asia which began *c.* 60 million years ago (e.g. Le Fort, 1996; Yin & Harrison, 2000). The range is presently characterized by high rates of seismicity and deformation (e.g. Yeats *et al.*, 1992), and widespread exposure of post-collisional, high-grade metamorphic rocks implies long-term, large-scale vertical transport. Over the past 30 years, numerous models have been proposed to explain the key petrological and tectonic features of the Himalayas (see Harrison *et al.*, 1999a; Hodges, 2000). These theories of crustal metamorphism have been widely exported to explain aspects of other mountain belts.

Most models for the evolution of the Himalayas centre around understanding the evolution of both the Main Central Thrust (MCT), an intracontinental shear zone located at the present-day topographic break in slope (e.g. Ni & Barazangi, 1984; Duncan *et al.*, 2003), and the South Tibet Detachment System (STDS), which roughly parallels the MCT along strike (Fig. 1). The STDS is regularly found in close association with Miocene-age High Himalayan leucogranites (e.g. Harrison *et al.*, 1995), which formed as a result of anatexis of the MCT hangingwall (e.g. Harris *et al.*, 1993). A 2–10 km thick MCT shear zone juxtaposes high-grade metamorphic gneisses (Greater Himalayan Crystallines) atop lower-grade metasedimentary rocks (Lesser Himalaya Formations).

Although the MCT has long been thought to be an early Miocene structure (e.g. Hodges *et al.*, 1996; Vannay & Hodges, 1996), rocks within the broad associated shear zone were recently reported to have experienced metamorphism later than previously thought (Harrison *et al.*, 1997a; Catlos *et al.*, 2001, 2002a). Th–Pb dating of small (*c.* 15 μm sized) monazite from rocks within the recrystallized MCT shear zone in central Nepal yields ages as young as *c.* 3 Ma. This paper presents U–Pb zircon and Th–Pb monazite ages and pressure–temperature (*P–T*) constraints from rocks from the Sikkim region of northern India (Fig. 2). The results have implications for the understanding of models proposed for the evolution of the range, as well as the general structural and metamorphic evolution of orogenic hinterlands, the geodynamic development of continental collisions, and the application of thermochronometric techniques in structural analysis.

GEOLOGICAL BACKGROUND

The MCT is generally thought to have been active subsequent to Late Cretaceous–Early Eocene

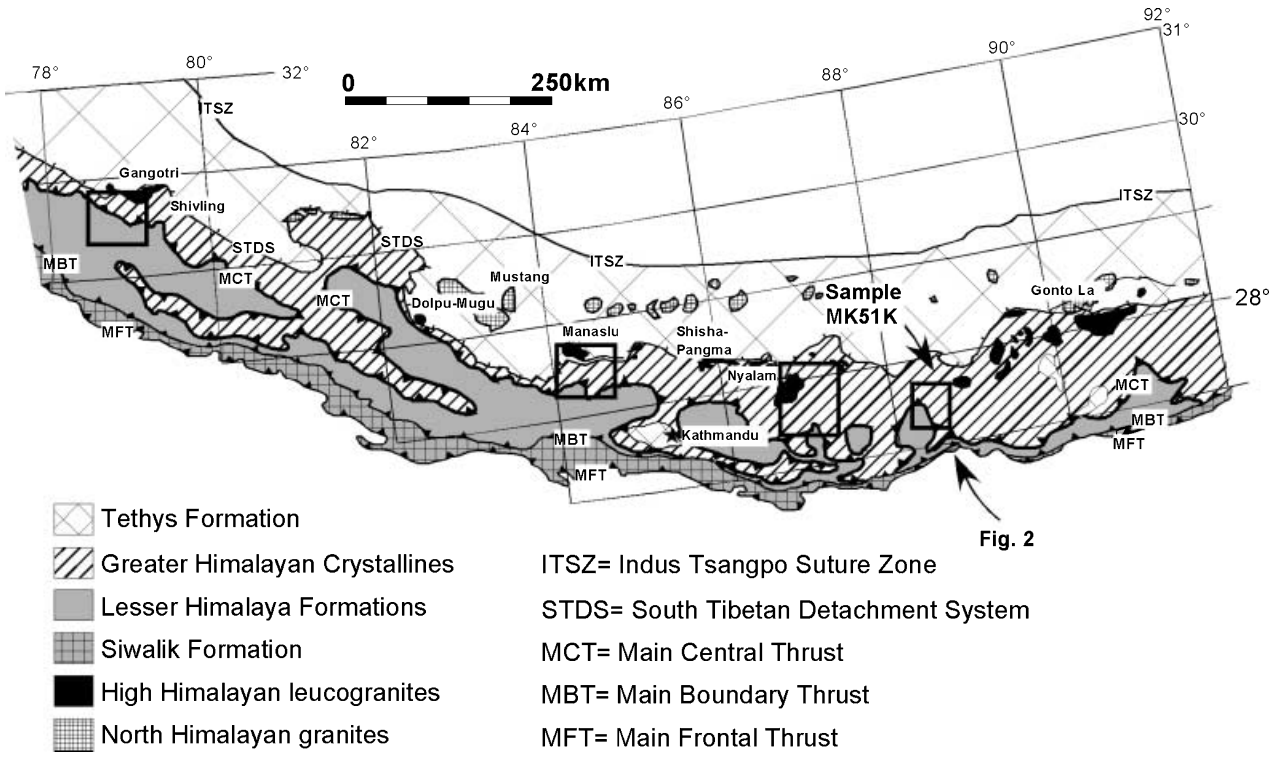

Fig. 1. Generalized geological map of the Himalayan range after Le Fort (1996). Boxes outline the areas where post-Early Miocene monazite ages have been found and are, from east to west: Sikkim, NE India (this paper; Fig. 2), Dudh Kosi–Everest transect, eastern Nepal (Catlos *et al*., 2002a); Annapurna–Manaslu–Ganesh region, central Nepal (Harrison *et al*., 1998; Catlos *et al*., 2001); and Garhwal Himalaya, India (Catlos *et al*., 2002a). Names of some of the High Himalayan and North Himalayan granite bodies are included for reference. Sample MK51K was collected at ~27°51′N and 88°50′E.

Indo-Asia collision (e.g. Le Fort, 1996; Yin & Harrison, 2000) as deformation shifted from the Indus–Tsangpo suture (Fig. 1) towards the foreland (e.g. the evolutionary model of Seeber & Gornitz, 1983). Although contraction appears to have broadly progressed towards the Himalayan foreland as activity shifted from the MCT during the Early Miocene (e.g. Hodges *et al*., 1996) to the Main Boundary Thrust (MBT) during the Late Miocene (e.g. Meigs *et al*., 1995), to the currently active Main Frontal Thrust (MFT, e.g. Yeats *et al*., 1992), monazite ages from the Lesser Himalaya in central Nepal and NW India (Harrison *et al*., 1997a; Catlos *et al*., 2001, 2002a) indicate that the hinterland thickened internally during the Late Miocene and Pliocene. The generality of this out-of-sequence thickening along strike of the range remains unknown because post-Early Miocene MCT movement may be restricted to certain regions (central Nepal, Harrison *et al*., 1997a; Catlos *et al*., 2001; eastern Nepal & NW India, Catlos *et al*., 2002a; see Stephenson *et al*., 2001).

The MCT footwall displays 'inverted metamorphism', an increase in metamorphic intensity towards higher structural levels (e.g. Ray, 1947). The single quantity speculated to constrain most tightly the possible heat sources responsible for the creation of this apparent inverted thermal gradient is the age of slip of the MCT (England *et al*., 1992). The presence of *c*. 6 Ma, and as young as *c*. 3 Ma, monazite ages from the apparent inverted metamorphic sequence in central Nepal suggests that thrusts within the footwall shear zone juxtaposed 'right-way-up' metamorphic sequences into their inverted position (Harrison *et al*., 1997a, 1998). A recent model based on structural observations in western Nepal and geochronological and thermobarometric constraints from central Nepal describes these thrusts as part of a Lesser Himalaya duplex system (Robinson *et al*., 2003). One of the requirements of this model is a progressive southward incorporation of the footwall slices. Thus, obtaining ages from the MCT footwall inverted metamorphic sequence from other regions within the Himalayas can test the validity of these hypotheses.

Post-collisional, Miocene-age High Himalayan leucogranites formed by anatexis of the Greater Himalayan Crystallines (e.g. Harris *et al*., 1993; Harrison *et al*., 1995) are generally found adjacent to, or cut by, the STDS (Fig. 1) (Harrison *et al*., 1999a,b; Hodges, 2000). Recognition of this geological relationship, together with geophysical data that suggest that the MCT and STDS could converge at depth

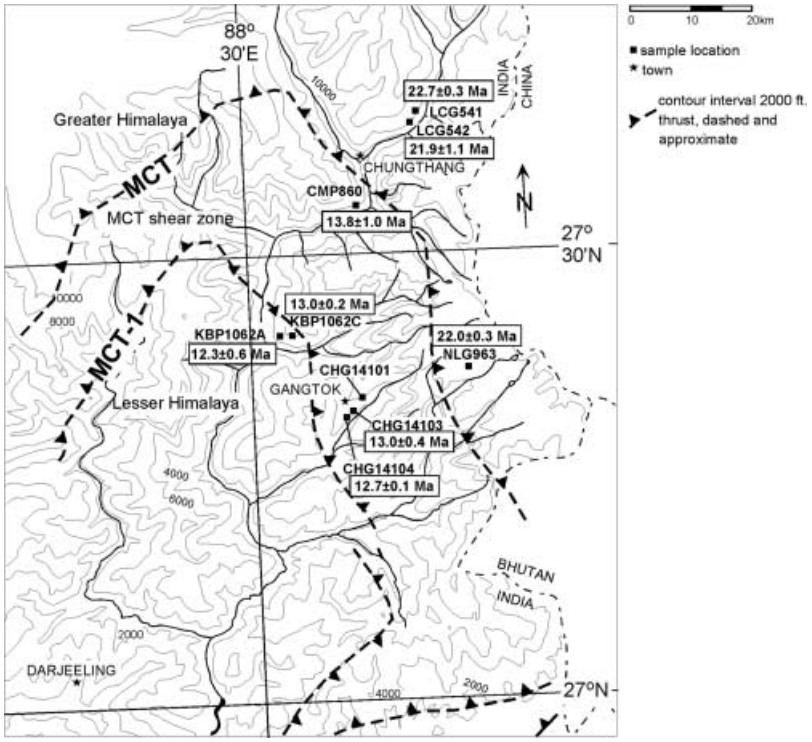

Fig. 2. Sample traverse map showing locations of rocks analyzed for monazite ages and *P–T* information. For a detailed geological map of the Sikkim Himalayas, refer to Dubey (1993), Mohan *et al.* (1989) and Ganguly *et al.* (2000). Placement of the bounds of the MCT shear zone (MCT and MCT-1) is based on structural observations and monazite ages.

(Nelson *et al.*, 1996), led to the suggestion that the Greater Himalayan Crystallines extruded as a coherent wedge due to simultaneous thrusting along the MCT and extension along the STDS (e.g. Hodges *et al.*, 1993). Greater Himalayan Crystallines monazite ages from central Nepal are generally inconsistent with synchronous MCT and STDS activity as monazite within the MCT shear zone are *c.* 20 Myr younger than those obtained from rocks at higher structural levels of the hangingwall (Catlos *et al.*, 2001). However, significant STDS slip and concomitant juxtaposition of rocks of contrasting metamorphic grade are not apparent in central Nepal (e.g. Bordet *et al.*, 1975; Fuchs *et al.*, 1988, 1999), thus the significance of this result may be overstated. Obtaining precise ages that constrain slip on these faults from regions in the Himalayas that are characterized by clear phases of movement on the MCT and STDS are key for testing the concept of Greater Himalayan wedge extrusion, as well as estimating slip and denudation rates and constraining factors involved in crustal melting, including the volume and rate of melt generation.

METHODS

Monazite and zircon analysis

This paper focuses on ion microprobe dating of two radiogenic-element-bearing minerals commonly found in Himalayan rocks: zircon ($ZrSiO_4$) and monazite ($CeLaThPO_4$). Zircon is stable under a broad range of crustal pressures and temperatures, and survives most geological processes (e.g. weathering, sedimentary transport, crustal melting and metamorphism) while being highly retentive of daughter products in the U–Pb decay system (e.g. Schneider *et al.*, 1999; Cherniak & Watson, 2001; Harrison *et al.*, 2002). Crystalline zircon does not reset U–Pb ages under metamorphic conditions, and thus is often used to provide information about events occurring early in Earth's history (e.g. Mojzsis & Harrison, 2002).

Monazite incorporates little or no Pb during crystallization while remaining relatively impervious to Pb loss at high crustal temperatures (Harrison *et al.*, 2002; Cherniak *et al.*, 2003). The mineral is resilient to radiation damage (Meldrum *et al.*, 1998), but can reset during certain geological events, thus recording information about complexly metamorphosed regions (Catlos *et al.*, 2002b). The stability field of monazite is only broadly known (Wing *et al.*, 2003), but the mineral generally forms in pelites under conditions coincident with garnet growth (*c.* 525 °C) from the breakdown of allanite, a rare-earth element (REE) bearing silicate mineral. Other proposed monazite-forming reactions include production from REE oxides and dissolution/reprecipitation of existing grains (e.g. Smith & Barreiro, 1990; Ayers *et al.*, 1999; Zhu & O'Nions, 1999).

All age measurements reported in this paper were obtained *in situ* (in thin section), except those for zircon and monazite grains separated from the Pauhunri leucogranite (MK51K), which were analyzed in an epoxy mount. Using an ion microprobe to date monazite in thin section preserves the grain of interest and its relationship to the textures of the rock. The reader is referred to Catlos *et al.* (2002b) for technical details of *in situ* Th–Pb monazite analysis, and Schneider *et al.* (1999) for U–Pb dating of zircon. The errors for all ages reported in this paper are 1 σ.

As seen in Figs 3 and 4, MK51K zircon and monazite are sub- to euhedal and range from 70 μm to 1 mm in length. Monazite grains dated in thin section are zoned and irregularly shaped, and range from 30 to 200 μm in length (e.g. Fig. 5). The O^- beam used to sputter isotopes of Th and Pb from the monazite grains was *c.* 30 μm in diameter, thus no attempt was made to date specific chemical zones. Multiple analyses could be made on the larger minerals, and in some cases core and rim analyses were taken from the zircon that showed distinct zoning in transmitted light.

Catlos *et al.* (2002b) outlined the approach used in this paper to use the monazite ages as a means to constrain a structural history, which is briefly summarized here. The ideal situation exists if monazite inclusions in garnet and matrix monazite yield ages

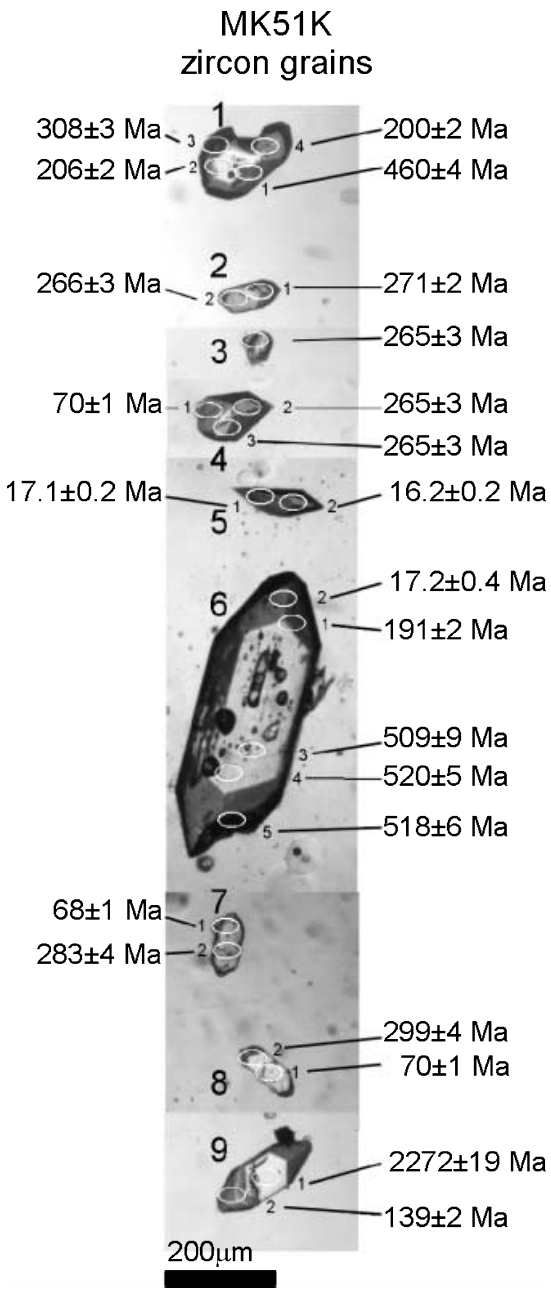

Fig. 3. Transmitted light images of MK51K zircon with ^{238}U–^{206}Pb age (± 1σ) indicated. The location of the ion microprobe spot is indicated by the circle with spot number. The number of the grain is indicated by the larger number. The scale bar is 200 μm. See Table 8 for detailed analyses.

consistent with a single population. Garnet can physically protect the monazite inclusion from Pb diffusion or reactions with fluids (Montel *et al.*, 2000), and can be used with other coexisting minerals in the sample to record the peak metamorphic *P–T* conditions or the *P–T* path. Thus, the age can be linked to a *P–T* point or a segment along a *P–T* path (see Catlos *et al.*, 2002a for an example).

However, questions arise when the ages of monazite within garnet and in the matrix are inconsistent with a single age. This scenario requires a more detailed scrutiny of the sample, typically including X-ray obtaining element garnet maps assessing the peak metamorphic

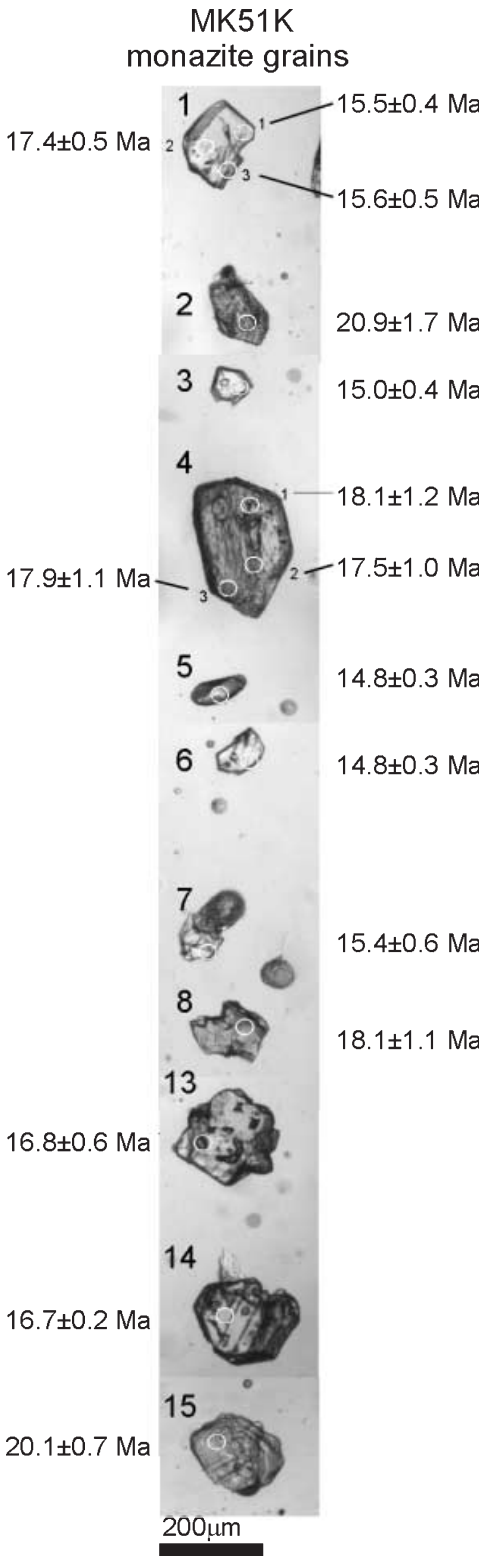

Fig. 4. Transmitted light images of MK51K monazite with ^{232}Th–^{208}Pb age (± 1σ) indicated. The location of the ion microprobe spot is indicated by the circle with analysis number. The scale bar is 200 μm. The average age of MK51K monazite (n = 15) is 17.0 Ma ± 0.8, MSWD = 8.5. See Table 9 for detailed analyses.

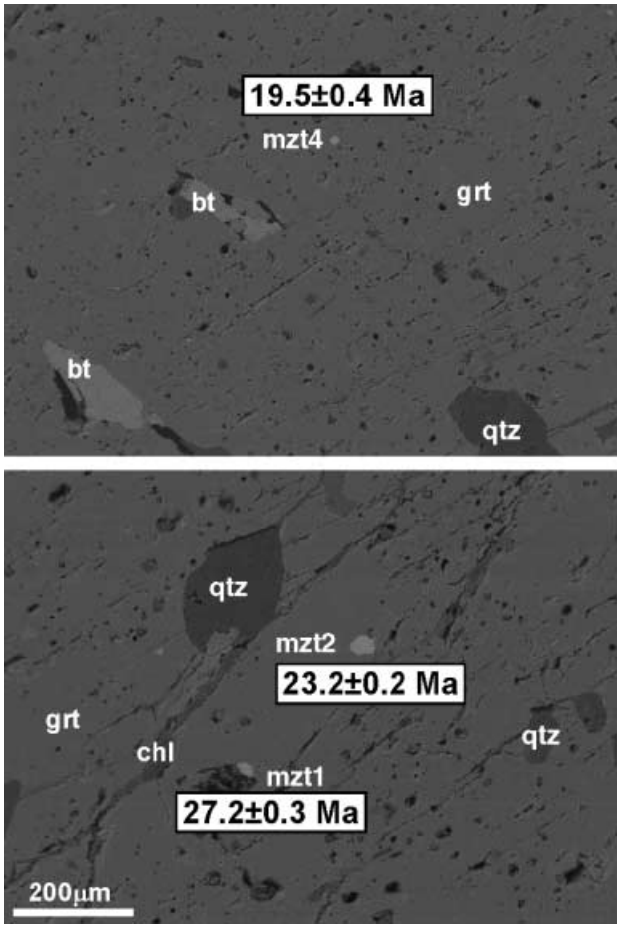

Fig. 5. Backscattered electron (BSE) image of Greater Himalayan Crystallines sample LCG541. All monazite in these images are inclusions in garnet, 'grt', and are indicated with grain number (mzt#) and age (± 1σ). See Table 1 for details of the age analyses. Other abbreviations include 'bt', biotite, 'qz', quartz, and 'chl', chlorite. The scale bar is applicable to both panels.

conditions and possible polymetamorphism or retrogression experienced by the rock, using other geochronological data from the region, including previous work or dating other minerals in the sample, evaluating any method-related uncertainty, and ascertaining possible monazite-producing reactions and evidence for fluid interaction.

Matrix monazite has been thought to be subject to Pb loss due to prolonged exposure to conditions above the closure temperature. In this case, *P–T* conditions from the garnet and matrix minerals can be used to discern the peak conditions achieved by the rock and the possible effect of Pb loss. However, it as yet unclear whether the concept of a closure temperature is readily applicable to monazite, as studies of Pb diffusion in monazite indicate a retentivity similar to that of zircon (Cherniak *et al*., 2000, 2003).

Overall, the structural location of the sample is key for deciphering the meaning of the mineral age. Our rocks were collected from coherent outcrops adjacent to the MCT or within a slightly deformed leucogranite in close proximity to the STDS (see below), thus the obtained ages can be reasonably confidently related to the timing of slip along these structures. However, tying the monazite age to a specific rock matrix fabric may be difficult because of the insolubility of the mineral during metamorphism. For example, when garnet grows, material necessary for growth is transported to the surface of the porphyroblast. We speculate that garnet may appear in rocks adjacent to the MCT via a continuous reaction involving chlorite breakdown [chlorite + quartz → garnet + H_2O]. Minerals adjacent to the garnet grain that do not participate in the reaction are removed by dissolution and diffusion or are overgrown and encompassed in the porphyroblast as a passive inclusion (e.g. Passchier & Trouw, 1996). The location of the monazite within the garnet is key textural evidence that links the monazite age to a specific *P–T* point or path. However, in the matrix of the rock, the fabric around the monazite grain may deform, but the monazite itself may not experience conditions sufficient enough to change shape, reset in age or physically dissolve and be transported to the section of the rock that records the specific deformation orientation. Although the monazite may be found within a specific deformation fabric, its age may not date the creation of that fabric.

Although some researchers advocate high-resolution compositional mapping of monazite grains to evaluate the presence of polymetamorphic growth, this approach is not taken in this paper. Monazite composition can be influenced by several factors, including the orientation of the crystal in the thin section, the transfer of elements from the breakdown of REE phases under changing *P–T* conditions, competitive crystallization among other REE phases, or replacement of an original grain during metamorphism (e.g. Cressey *et al*., 1999; Zhu & O'Nions, 1999; Townsend *et al*., 2000; Pyle *et al*., 2001).

Sample description and thermobarometric methods

Rocks were collected from the Lesser Himalaya (KBP1062A and KBP1062C) and MCT shear zone (CMP860, CHG14104 and CHG14103), and the Greater Himalayan Crystallines (NLG963, LCG542 and LCG541) (Fig. 2). A sample was also collected from the Pauhunri leucogranite (MK51K: Edwards *et al*., 2002). Lesser Himalaya samples have garnet + biotite + staurolite + muscovite + plagioclase + chlorite + ilmenite + apatite + monazite + zircon + xenotime + quartz. MCT shear zone rock CMP860 has garnet + biotite + sillimanite + muscovite + plagioclase + chlorite + ilmenite + monazite + tourmaline + zircon + apatite + allanite + quartz, whereas samples CHG14103 and CHG14104 have garnet + biotite + staurolite + muscovite + plagioclase + chlorite + ilmenite + zircon + monazite ± xenotime ± apatite ± allanite + quartz. Greater Himalayan Crystallines NLG963 has garnet + biotite + sillimanite + muscovite + plagioclase + chlorite + ilmenite + monazite + zircon + quartz. The other Greater Himalayan Crystallines rocks have a similar assemblage, but LCG542 has kyanite with fibrillose sillimanite overgrowths and LCG541 lacks plagioclase.

Sikkim rocks chosen for peak *P–T* calculations are garnet-bearing assemblages containing biotite ± chlorite ± staurolite as the major Fe–Mg minerals. Chlorite is commonly found near or in contact with the garnet, but garnet crystals with textures suggestive of significant retrogression were avoided for thermobarometric analysis. Data used to calculate the *P–T* conditions include electron microprobe mineral compositions and garnet X-ray element maps. The maps were used to evaluate garnet zoning patterns qualitatively and ensure that areas chosen for quantitative analysis best estimate the *P–T* conditions recorded by each assemblage (e.g. Kohn & Spear, 2001).

Table 1. *In situ* monazite age results from the Greater Himalayan Crystallines, Sikkim.

Sample[a] (grain–spot)	Monazite location[b]	Age (Ma) (± σ)	ThO_2^+/Th^+[c] (± σ)	^{208}Pb (%)[d] (± σ)	$^{208}Pb^*/Th^+$[e] (± σ)
LCG542					
7–1	m	25.6 (0.3)	3.268 (0.034)	94.9 (0.8)	1.266E−03 (1.624E−05)
3–1	m	23.2 (1.3)	2.836 (0.025)	41.1 (2.2)	1.150E−03 (6.362E−05)
2–1	m	21.5 (0.6)	3.570 (0.049)	86.5 (1.2)	1.063E−03 (2.745E−05)
1–1	m	20.3 (0.8)	3.631 (0.039)	76.9 (2.2)	1.004E−03 (3.863E−05)
6–1	m	18.8 (0.5)	3.863 (0.034)	82.1 (1.7)	9.316E−04 (2.347E−05)
LCG542 calibration: $(0.099 \pm 0.001)x + (0.881 \pm 0.037)$; $r^2 = 0.948$; $ThO_2^+/Th^+ = 4.028 \pm 0.668$[f]					
LCG541					
1–1	i	27.2 (0.3)	4.567 (0.027)	95.2 (0.3)	1.348E−03 (1.470E−05)
2–1	i	23.2 (0.2)	3.861 (0.014)	96.5 (0.3)	1.150E−03 (1.025E−05)
5–1	i	21.2 (0.2)	4.475 (0.010)	95.9 (0.4)	1.048E−03 (9.319E−06)
3–1	i	22.3 (0.2)	3.744 (0.015)	94.4 (0.3)	1.105E−03 (1.108E−05)
4–1	i	19.5 (0.4)	4.280 (0.012)	90.1 (1.4)	9.668E−04 (2.210E−05)
LCG541 calibration: $(0.085 \pm 0.002)x + (1.803 \pm 0.047)$; $r^2 = 0.976$; $ThO_2^+/Th^+ = 4.000 \pm 0.491$[f]					
NLG963					
1–1	m	19.2 (0.4)	3.559 (0.020)	92.7 (0.9)	9.519E−04 (2.085E−05)
8–1	m	29.0 (0.4)	3.783 (0.013)	95.4 (0.5)	1.437E−03 (1.771E−05)
3–1	m	18.4 (0.3)	3.640 (0.014)	92.3 (0.8)	9.121E−04 (1.495E−05)
NLG963 calibration: $(0.049 \pm 0.002)x + (2.184 \pm 0.085)$; $r^2 = 0.991$; $ThO_2^+/Th^+ = 3.946 \pm 0.276$[f]					

[a] Nomenclature indicates the grain and spot, respectively, of the analyzed monazite.
[b] Monazite inclusion in garnet is designated as 'i', whereas 'm' indicates a matrix grain.
[c] Measured ratio in sample.
[d] Percentage radiogenically derived ^{208}Pb.
[e] Corrected sample ratio assuming $^{208}Pb/^{204}Pb = 39.5 \pm 0.1$ (Stacey & Kramers, 1975).
[f] Calibration information: sample name, best fit of the calibration to the equation of a line (slope*x + intercept) with ± 1σ uncertainty, correlation (r^2), and range of ThO_2^+/Th^+ (± 1σ) measured using monazite 554 (e.g. Harrison *et al.*, 1999b). Ideally, the unknown ThO_2^+/Th^+ lies within the ThO_2^+/Th^+ range defined by the standard.

Table 2. *In situ* monazite age results from the MCT shear zone, Sikkim.

Sample[a] (grain–spot)	Monazite location[b]	Age (Ma) (± σ)	ThO_2^+/Th^+[c] (± σ)	^{208}Pb (%)[d] (± σ)	$^{208}Pb^*/Th^+$[e] (± σ)
CMP860					
7–1	i	20.5 (0.6)	3.411 (0.018)	92.1 (1.2)	1.015E−03 (2.996E−05)
8–1	i	13.8 (0.8)	3.099 (0.009)	78.9 (2.9)	6.833E−04 (4.095E−05)
3–1	m	19.7 (0.8)	3.299 (0.013)	80.4 (2.1)	9.740E−04 (3.896E−05)
1–3	m	14.3 (0.7)	3.173 (0.013)	87.0 (2.0)	7.055E−04 (3.385E−05)
4–1	m	12.7 (0.4)	3.557 (0.017)	84.4 (1.8)	6.277E−04 (1.885E−05)
1–1	m	11.2 (0.3)	3.768 (0.014)	86.7 (1.6)	5.549E−04 (1.264E−05)
1–2	m	10.3 (0.2)	3.800 (0.018)	87.5 (1.7)	5.117E−04 (1.224E−05)
CMP860 Calibration 1: $(0.049 \pm 0.002)x + (2.184 \pm 0.085)$; $r^2 = 0.991$; $ThO_2^+/Th^+ = 3.946 \pm 0.276$[f]					
10–1	i	11.2 (0.3)	3.505 (0.019)	81.8 (1.9)	5.543E−04 (1.565E−05)
9–1	i	10.8 (0.3)	3.558 (0.054)	85.3 (1.6)	5.362E−04 (1.359E−05)
CMP860 calibration 2: $(0.099 \pm 0.001)x + (0.881 \pm 0.037)$; $r^2 = 0.948$; $ThO_2^+/Th^+ = 4.028 \pm 0.668$[f]					
CHG14103					
2–1	m	13.8 (0.5)	3.328 (0.020)	90.1 (1.1)	6.826E−04 (2.310E−05)
6–1	m	13.7 (0.5)	3.370 (0.023)	85.0 (1.6)	6.784E−04 (2.518E−05)
4–1	m	13.2 (0.5)	3.520 (0.031)	88.2 (1.6)	6.537E−04 (2.268E−05)
1–1	m	12.9 (0.4)	3.380 (0.015)	92.1 (0.9)	6.380E−04 (1.866E−05)
3–1	m	12.2 (0.4)	3.556 (0.035)	87.5 (1.3)	6.035E−04 (2.099E−05)
5–1	m	11.9 (0.3)	3.551 (0.030)	87.3 (1.4)	5.891E−04 (1.699E−05)
CHG14103 calibration: $(0.049 \pm 0.002)x + (2.184 \pm 0.085)$; $r^2 = 0.991$; $ThO_2^+/Th^+ = 3.946 \pm 0.276$[f]					
CHG14104					
9–1	i	13.1 (0.2)	4.631 (0.031)	93.0 (0.9)	6.464E−04 (1.049E−05)
8–1	i	12.4 (0.1)	4.494 (0.010)	94.0 (0.5)	6.142E−04 (6.418E−06)
10–1	i	12.2 (0.2)	4.728 (0.010)	93.2 (1.0)	6.056E−04 (8.925E−06)
3–1	m	14.3 (0.1)	3.697 (0.008)	90.0 (0.6)	7.099E−04 (7.026E−06)
7–1	m	13.2 (0.1)	4.266 (0.008)	95.1 (0.4)	6.521E−04 (5.612E−06)
11–1	m	13.2 (0.1)	3.996 (0.009)	94.4 (0.5)	6.543E−04 (5.128E−06)
2–1	m	12.8 (0.1)	4.312 (0.010)	95.8 (0.3)	6.330E−04 (5.360E−06)
4–1	m	12.3 (0.1)	4.436 (0.009)	93.8 (0.5)	6.098E−04 (5.845E−06)
6–1	m	12.1 (0.1)	4.623 (0.012)	93.6 (0.5)	5.985E−04 (6.555E−06)
1–1	m	11.5 (0.1)	4.367 (0.009)	93.8 (0.5)	5.709E−04 (5.474E−06)
CHG14104 calibration: $(0.085 \pm 0.002)x + (1.803 \pm 0.047)$; $r^2 = 0.976$; $ThO_2^+/Th^+ = 4.000 \pm 0.491$[f]					

[a] Nomenclature indicates the grain and spot, respectively, of the analyzed monazite.
[b] Monazite inclusion in garnet is designated as 'i', whereas 'm' indicates a matrix grain.
[c] Measured ratio in sample.
[d] Percentage radiogenically derived ^{208}Pb.
[e] Corrected sample ratio assuming $^{208}Pb/^{204}Pb = 39.5 \pm 0.1$ (Stacey & Kramers, 1975).
[f] Calibration information: sample name, best fit of the calibration to the equation of a line (slope*x + intercept) with ± 1σ uncertainty, correlation (r^2), and range of ThO_2^+/Th^+ (± 1σ) measured using monazite 554 (e.g. Harrison *et al.*, 1999b). Ideally, the unknown ThO_2^+/Th^+ lies within the ThO_2^+/Th^+ range defined by the standard. Two analysis sessions were used to date monazite from sample CMP860.

Table 3. *In situ* monazite age results from the Lesser Himalaya, Sikkim.

Sample[a] (grain–spot)	Monazite location[b]	Age (Ma) ($\pm \sigma$)	ThO_2^+/Th^+[c] ($\pm \sigma$)	^{208}Pb (%)[d] ($\pm \sigma$)	$^{208}Pb^*/Th^+$[e] ($\pm \sigma$)
KBP1062C					
1–1	i	12.2 (0.1)	4.493 (0.022)	93.1 (0.5)	6.043E−04 (6.992E−06)
3–1	i	11.9 (0.2)	4.518 (0.016)	92.7 (1.0)	5.863E−04 (8.256E−06)
4–1	i	11.6 (0.2)	3.749 (0.009)	80.1 (1.4)	5.759E−04 (1.166E−05)
2–1	i	11.5 (0.2)	4.410 (0.029)	79.4 (1.0)	5.671E−04 (9.564E−06)
5–1	m	18.3 (0.1)	3.876 (0.007)	93.7 (0.3)	9.076E−04 (6.868E−06)
7–1	m	12.9 (0.2)	3.928 (0.012)	90.7 (0.6)	6.369E−04 (9.210E−06)
6–1	m	12.5 (0.3)	4.086 (0.021)	84.5 (1.1)	6.170E−04 (1.486E−05)
KBP1062C Calibration: $(0.085 \pm 0.002)x + (1.803 \pm 0.047)$; $r^2 = 0.976$; $ThO_2^+/Th^+ = 4.000 \pm 0.491$[f]					
KBP1062A					
5–1[f]	i	12.7 (0.3)	4.170 (0.016)	88.9 (2.0)	6.275E−04 (1.562E−05)
10–1[f]	i	12.1 (0.6)	3.343 (0.034)	64.9 (2.8)	5.973E−04 (3.084E−05)
9–1[f]	i	12.0 (0.3)	3.930 (0.024)	85.8 (1.8)	5.951E−04 (1.466E−05)
2–1	m	14.2 (1.1)	3.015 (0.022)	55.3 (3.8)	7.001E−04 (5.443E−05)
3–1	m	12.6 (0.5)	2.779 (0.034)	66.1 (2.2)	6.248E−04 (2.625E−05)
6–1	m	11.9 (0.4)	3.735 (0.021)	77.1 (2.4)	5.896E−04 (2.104E−05)
1–1	m	10.5 (0.6)	2.886 (0.023)	56.5 (2.8)	5.211E−04 (3.006E−05)
KBP1062A Calibration: $(0.099 \pm 0.001)x + (0.881 \pm 0.037)$; $r^2 = 0.948$; $ThO_2^+/Th^+ = 4.028 \pm 0.668$[f]					

[a] Nomenclature indicates the grain and spot, respectively, of the analyzed monazite.
[b] Monazite inclusion in garnet is designated as 'i', whereas 'm' indicates a matrix grain.
[c] Measured ratio in sample.
[d] Percentage radiogenically derived ^{208}Pb.
[e] Corrected sample ratio assuming $^{208}Pb/^{204}Pb = 39.5 \pm 0.1$ (Stacey & Kramers, 1975).
[f] Calibration information: sample name, best fit of the calibration to the equation of a line (slope*x + intercept) with $\pm 1\sigma$ uncertainty, correlation (r^2), and range of ThO_2^+/Th^+ ($\pm 1\sigma$) measured using monazite 554 (e.g. Harrison *et al.*, 1999b). Ideally, the unknown ThO_2^+/Th^+ lies within the ThO_2^+/Th^+ range defined by the standard.

Thermometer and barometer calibrations were applied using the garnet and matrix mineral compositions. Garnet–biotite thermometry (Ferry & Spear, 1978; Berman, 1990) and garnet–plagioclase–biotite–muscovite barometry (Hoisch, 1990) were used to constrain temperature and pressure. Different thermobarometric calibrations change estimated conditions by $\pm$ 25 °C and $\pm$ 0.1 GPa, but overall trends are unaltered. A temperature only was calculated for Greater Himalayan Crystallines LCG541 because the rock lacked plagioclase.

Table 4. Compositions used to estimate LCG541 temperature.

	Grt[a]		Bt[b]	
SiO_2	37.4	38.1	35.8	36.1
Al_2O_3	21.6	21.6	17.4	17.5
MnO	1.1	1.0	–[c]	0.1
MgO	5.8	5.7	12.0	11.0
CaO	2.2	2.2	–	–
Na_2O	–	–	0.2	0.1
FeO	31.4	31.4	16.7	17.4
TiO_2	–	–	3.8	3.6
Cr_2O_3	–	0.1	–	0.1
K_2O	–	–	8.9	9.2
Total	100	100	95	95
Si	2.97	3.00	5.40	5.45
Al	2.02	2.00	3.09	3.11
Mn	0.07	0.07	< 0.01	0.01
Mg	0.69	0.67	2.69	2.49
Ca	0.19	0.19	< 0.01	< 0.01
Na	< 0.01	< 0.01	0.07	0.04
Fe	2.08	2.06	2.11	2.20
Ti	< 0.01	< 0.01	0.43	0.41
Cr	< 0.01	0.01	< 0.01	0.01
K	< 0.01	< 0.01	1.71	1.78
Total	8.0	8.0	15.5	15.5

[a] Rim compositions normalized to 12 oxygen. See Fig. 8 for analysis location.
[b] Matrix compositions normalized to 22 oxygen.
[c] '–', analyzed but not detected.

P–T–t CONSTRAINTS ON MCT SLIP

Tables 1–3 report details of the *in situ* monazite age data, and Tables 4–7 report the compositional data used to calculate the *P–T* conditions. Greater

Table 5. Compositions used to estimate CMP860 *P–T* conditions.

	Grt[a]		Bt[b]		Ms[b]		Plag[c]	
SiO_2	37.8	37.8	35.2	35.3	46.6	46.7	58.3	59.9
Al_2O_3	20.9	20.9	18.5	18.8	37.4	36.6	26.3	25.4
MnO	0.3	–[d]	0.1	0.1	–	–	–	–
MgO	3.4	2.9	7.9	8.3	0.5	0.5	–	–
CaO	2.6	4.1	–	–	–	–	7.9	6.8
Na_2O	–	–	0.2	0.2	0.8	0.8	6.7	7.5
FeO	35.6	34.6	20.3	20.8	1.5	1.5	0.1	–
TiO_2	–	0.1	2.3	2.2	0.4	0.5	–	–
Cr_2O_3	0.1	–	–	–	–	0.1	0.1	–
K_2O	–	–	9.6	9.6	9.5	9.4	0.1	0.1
Total	101	100	94	95	97	96	100	100
Si	3.01	3.02	5.46	5.42	6.07	6.13	2.61	2.67
Al	1.97	1.97	3.39	3.40	5.75	5.66	1.39	1.33
Mn	0.02	< 0.01	0.01	0.02	< 0.01	< 0.01	< 0.01	< 0.01
Mg	0.40	0.35	1.82	1.90	0.10	0.10	< 0.01	< 0.01
Ca	0.22	0.35	< 0.01	< 0.01	< 0.01	< 0.01	0.38	0.32
Na	< 0.01	< 0.01	0.05	0.05	0.21	0.20	0.59	0.65
Fe	2.37	2.31	2.63	2.67	0.16	0.16	< 0.01	< 0.01
Ti	< 0.01	< 0.01	0.27	0.25	0.04	0.05	< 0.01	< 0.01
Cr	< 0.01	< 0.01	0.01	< 0.01	< 0.01	0.01	< 0.01	< 0.01
K	< 0.01	< 0.01	1.90	1.88	1.58	1.57	0.01	0.01
Total	8.0	8.0	15.5	15.6	13.9	13.9	5.0	5.0

[a] Rim compositions normalized to 12 oxygen. See Fig. 10 for analysis locations.
[b] Matrix compositions normalized to 22 oxygen.
[c] Matrix compositions normalized to 8 oxygen.
[d] '–', analyzed but not detected.

Himalayan Crystallines samples LCG541, LCG542 and NLG963 monazite grains record Early Miocene ages, consistent with the timing of MCT slip elsewhere (e.g. Hodges *et al.*, 1996; Catlos *et al.*, 2001, 2002a). For example, matrix monazite in sample NLG963 average 22.2 ± 0.4 Ma, whereas matrix grains in LCG542 average 21.9 ± 0.7 Ma. LCG541 collected near LCG542 has a garnet that records 675 ± 25 °C and contains monazite inclusions that average 22.7 ± 0.3 Ma (Table 1, Figs 5 & 6). The assemblage contains sillimanite, and a sample collected near this rock (LCG542) contains kyanite and sillimanite, thus we speculate that the pressure conditions for LCG541 could be conservatively estimated from 6 to 8.5 kbar. Conditions previously estimated for other Greater Himalayan Crystallines samples range from 600 to 700 °C and 4 to 8 kbar (see Lal *et al.*, 1981; Mohan *et al.*, 1989; Dubey, 1993; Neogi *et al.*, 1998), resembling the LCG541 thermal conditions. Any discrepancies could reflect sample location, different calibrations used, or issues with the thermobarometric methods (Kohn & Spear, 2001).

The LCG541 garnet has an inclusion-filled core, containing small grains of monazite, quartz, ilmenite and biotite, with an inclusion-free rim (Fig. 7). Cracks filled with chlorite extend across the grain. The LCG541 garnet may be diffusionally homogenized, with flat spessartine profile (0.023 ± 0.002 mole fraction, 80 analyses) and increased Fe/(Fe + Mg) content from core to rim (0.68–0.72). The garnet displays patchy Ca zoning that does not follow the pattern outlined by the inclusions and with higher Ca concentrations in the core (0.04–0.09 mole fraction grossular). Overall, the LCG541 garnet elemental distribution is consistent with those mapped from the Greater Himalayan Crystallines elsewhere (e.g. Davidson *et al.*, 1997; Catlos *et al.*, 2001).

MCT shear zone rock CMP860 (650 ± 25 °C, 6 ± 1 kbar; Fig. 6) has monazite inclusions in garnet

Table 6. Compositions used to estimate CHG14103 *P–T* conditions.

	Grt[a]		Bt[b]		Ms[b]		Plag[c]	
SiO_2	37.2	37.2	34.7	34.9	47.3	46.7	63.7	63.2
Al_2O_3	20.9	20.8	18.9	18.6	36.0	37.0	23.9	24.3
MnO	0.2	0.1	–[d]	0.1	–	–	–	–
MgO	2.7	2.5	10.2	9.3	0.6	0.5	–	–
CaO	3.7	3.4	–	–	–	–	4.9	5.1
Na_2O	–	–	0.3	0.3	1.5	1.4	8.9	7.1
FeO	35.1	35.9	20.6	19.8	1.6	1.3	–	–
TiO_2	–	–	1.7	1.8	0.7	0.6	0.1	–
Cr_2O_3	0.1	–	–	–	0.1	–	–	–
K_2O	–	–	8.0	9.2	9.1	9.0	0.1	0.1
Total	100	100	95	94	97	97	102	100
Si	3.00	3.00	5.32	5.41	6.16	6.09	2.77	2.78
Al	1.99	1.98	3.43	3.39	5.53	5.69	1.23	1.26
Mn	0.01	0.01	0.01	0.01	< 0.01	< 0.01	< 0.01	< 0.01
Mg	0.32	0.30	2.34	2.14	0.12	0.09	< 0.01	< 0.01
Ca	0.32	0.30	< 0.01	< 0.01	< 0.01	< 0.01	0.23	0.24
Na	< 0.01	< 0.01	0.10	0.10	0.37	0.36	0.75	0.60
Fe	2.36	2.42	2.64	2.56	0.17	0.15	< 0.01	< 0.01
Ti	< 0.01	< 0.01	0.20	0.21	0.06	0.06	< 0.01	< 0.01
Cr	< 0.01	< 0.01	< 0.01	< 0.01	0.01	< 0.01	< 0.01	< 0.01
K	< 0.01	< 0.01	1.56	1.82	1.51	1.50	0.01	0.01
Total	8.0	8.0	15.6	15.6	13.9	13.9	5.0	4.9

[a] Rim compositions normalized to 12 oxygen.
[b] Matrix compositions normalized to 22 oxygen.
[c] Matrix compositions normalized to 8 oxygen.
[d] '–', analyzed but not detected.

Table 7. Compositions used to estimate KBP1062A *P–T* conditions.

	Grt[a]		Bt[b]		Ms[b]		Plag[c]	
SiO_2	37.8	37.6	35.9	36.0	46.5	46.8	66.3	66.4
Al_2O_3	21.2	21.3	19.1	19.0	36.6	37.1	22.2	22.4
MnO	0.3	0.5	0.1	0.1	–[d]	0.1	–	–
MgO	3.6	3.7	9.3	9.8	0.4	0.4	–	–
CaO	1.5	1.4	–	–	–	–	2.9	3.1
Na_2O	–	–	0.4	0.3	1.7	1.7	9.9	9.6
FeO	36.2	36.0	19.2	19.7	1.1	1.3	–	–
TiO_2	–	–	2.1	1.8	0.5	0.5	–	–
Cr_2O_3	–	–	0.1	–	–	0.1	–	–
K_2O	–	–	9.1	9.6	8.9	8.9	0.1	0.1
Total	101	101	95	96	96	97	102	102
Si	3.01	3.00	5.44	5.43	6.12	6.09	2.87	2.87
Al	1.99	2.00	3.43	3.38	5.66	5.69	1.13	1.14
Mn	0.02	0.03	0.01	0.01	< 0.01	0.01	< 0.01	< 0.01
Mg	0.43	0.44	2.10	2.20	0.09	0.09	< 0.01	< 0.01
Ca	0.13	0.12	< 0.01	< 0.01	< 0.01	< 0.01	0.13	0.14
Na	< 0.01	< 0.01	0.10	0.10	0.44	0.43	0.83	0.80
Fe	2.41	2.40	2.44	2.48	0.12	0.14	< 0.01	< 0.01
Ti	< 0.01	< 0.01	0.23	0.21	0.05	0.05	< 0.01	< 0.01
Cr	< 0.01	< 0.01	0.01	< 0.01	< 0.01	0.01	< 0.01	< 0.01
K	< 0.01	< 0.01	1.76	1.84	1.49	1.47	0.01	0.01
Total	8.0	8.0	15.5	15.6	14.0	14.0	5.0	5.0

[a] Rim compositions normalized to 12 oxygen. See Fig. 13 for analysis locations.
[b] Matrix compositions normalized to 22 oxygen.
[c] Matrix compositions normalized to 8 oxygen.
[d] '–', analyzed but not detected.

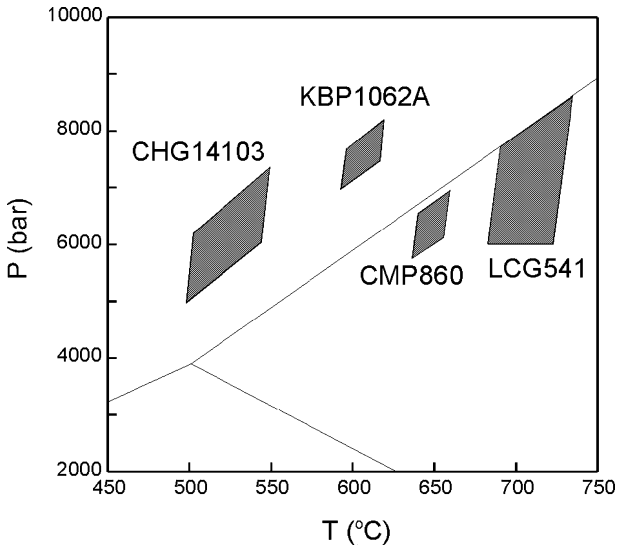

Fig. 6. *P–T* diagram of Lesser Himalaya (KBP1062A), MCT shear zone (CMP860 and CHG14103), and Greater Himalayan Crystallines (LCG541) samples. Lines denote the aluminosilicate stability fields. See text for an explanation of the baric conditions estimated for LCG541. See Tables 4–7 for mineral compositions used to estimate the *P–T* conditions.

that range from 20.5 ± 0.6 to 10.8 ± 0.3 Ma (Table 2, Fig. 8). Many garnet grains in this sample are skeletal and fragmented and contain inclusions of quartz, apatite, allanite, monazite, biotite, quartz and plagioclase (Fig. 8). The garnet used to calculate the *P–T* conditions, however, has a coherent rim but fragmented interior. The quartz and ilmenite inclusions within this garnet are not continuous with the overall foliation of the rock. The age distribution suggests that the sample went through a minimum of two monazite-forming reactions during the Miocene (*c*. 20 Ma) and Late Miocene (14–10 Ma). As inclusions of both ages are found in garnet, a mineral that armours monazite against daughter product loss (e.g. Montel *et al*., 2000), we expected the garnet to record a minimum two-stage metamorphic history in its zoning profile. The garnet is diffusively zoned or experienced retrograde garnet resorption (e.g. Florence & Spear, 1991), as seen by the increase at the rim in MnO (*c*. 0.05 to 2.8 wt%) and Fe/(Fe + Mg) (from 0.85 to 0.90) (Fig. 9). However, the garnet displays two broad increases in pyrope from core to rim that appear roughly to mirror decreases in grossular, leading to the irregular compositional traverse seen in Fig. 9, which are consistent overall with a change in metamorphic history or mineral assemblage during growth.

Further support for our hypothesis that monazite grains in CMP860 record their crystallization age is given by similar monazite ages found in rocks collected within the MCT shear zone and further south that

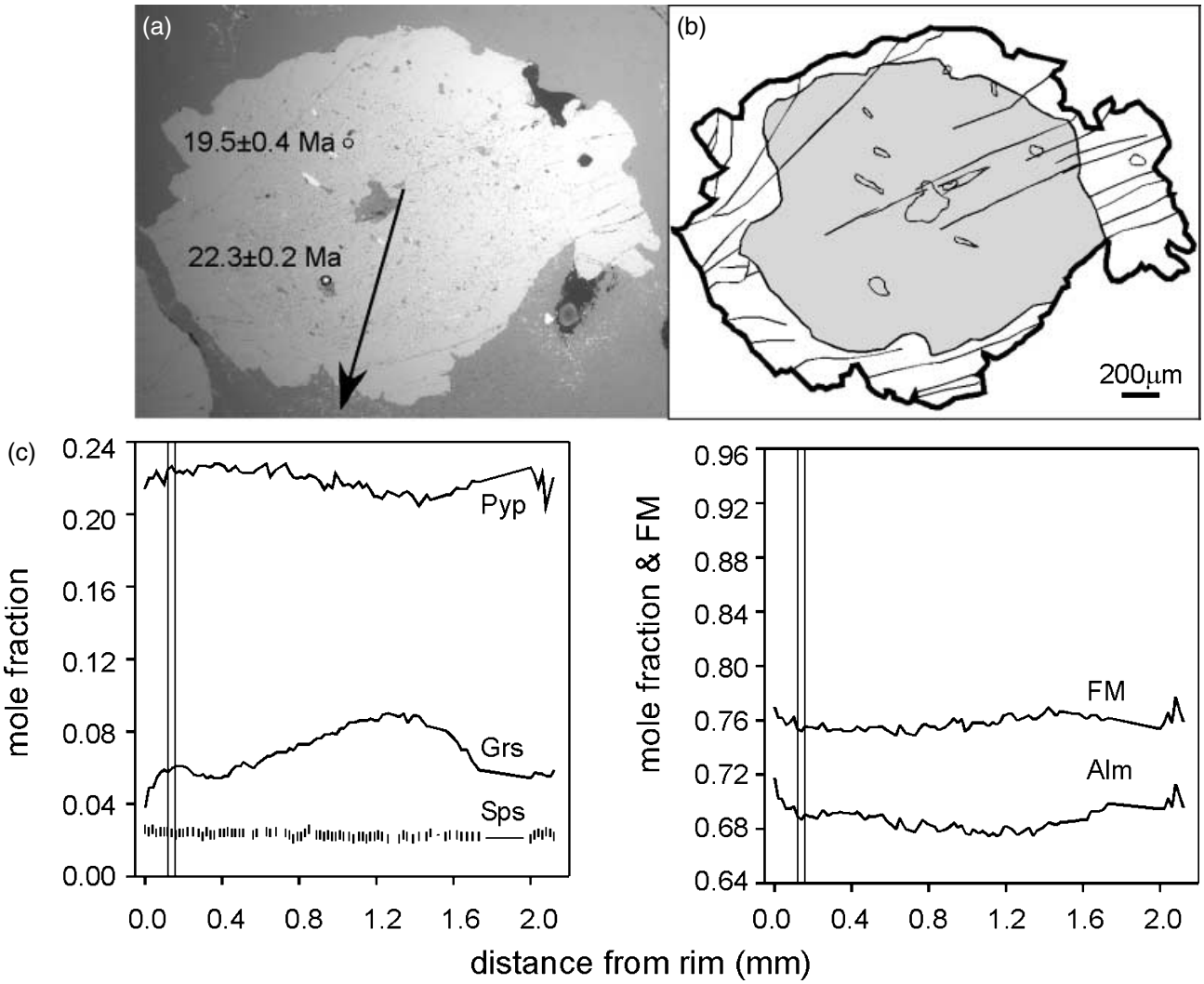

Fig. 7. (a) LCG541 garnet BSE image; (b) map of inclusion pattern and cracks; and (c) zoning profiles of mole fraction pyrope (Pyp), grossular (Grs), spessartine (Sps), Fe/(Fe + Mg) (FM) and almandine (Alm). The arrow in the BSE image is the approximate path where compositional analyses were taken, whereas the circles encompass dated monazite grains 3 and 4 (see also Fig. 5). See Table 1 for details of the age analyses. The shaded area in (b) outlines the inclusion-filled core of the garnet. Tick marks on the spessartine profile in (c) show the position of each analysis; the length of each tick has no statistical significance. The longer vertical lines in the lower zoning profiles are positions of compositions used for *P–T* calculations; see Table 4 for numerical values.

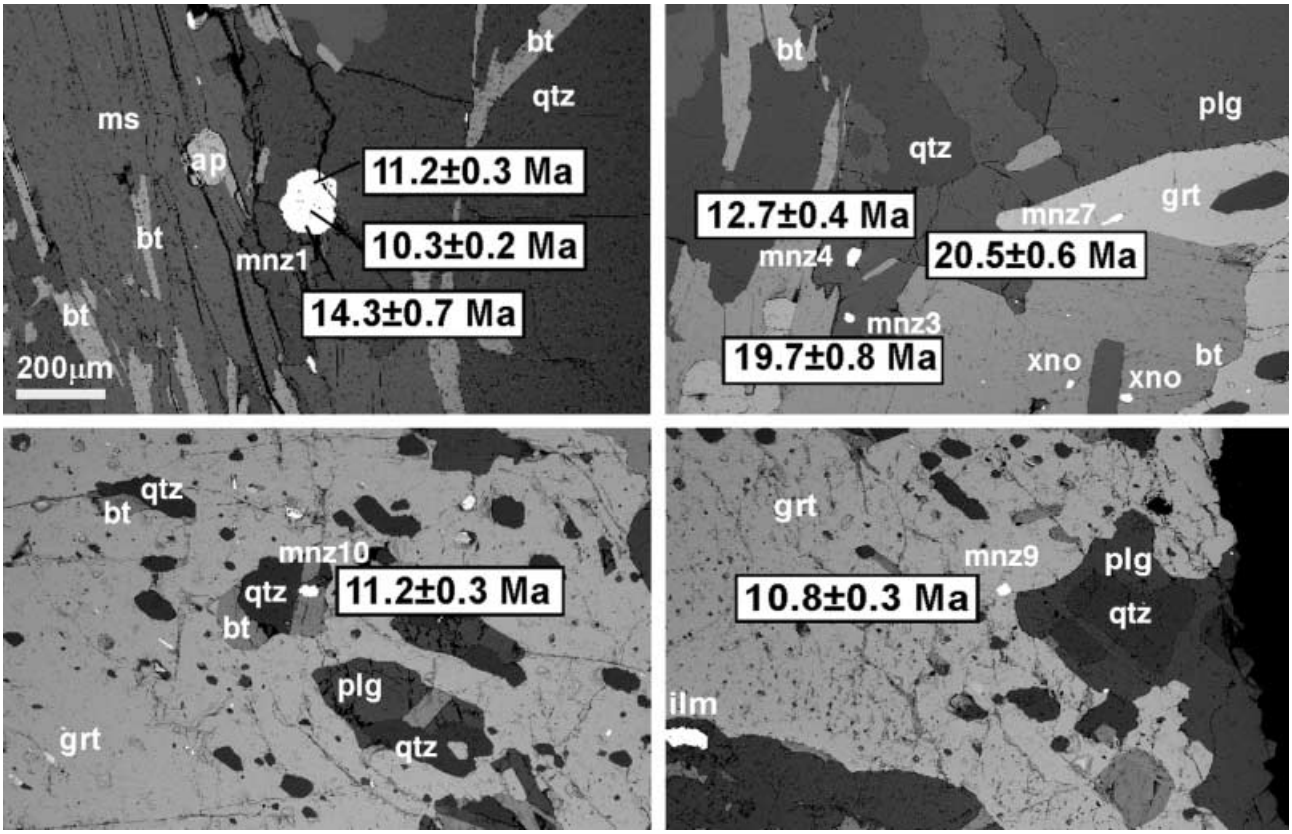

Fig. 8. BSE images of the Lesser Himalaya MCT shear zone rock CMP860. All dated monazite are indicated with grain number (mnz#) and age (± 1σ). See Table 2 for details of the age analyses. Other abbreviations include 'grt', garnet, 'bt', biotite, 'qtz', quartz, 'chl', chlorite, 'plg', plagioclase, 'ap', apatite, 'ilm', ilmenite and 'xno', xenotime. The scale bar is applicable to all figures.

experienced lower thermal conditions, but similar or higher pressures. For example, sample CHG14103 (525 ± 25 °C; 6 ± 1 kbar; Fig. 6) has 12–14 Ma inclusions in staurolite (Fig. 10), whereas CHG14104 has 12–13 Ma monazite inclusions in garnet (Table 2). The garnet in CHG14103 (Figs 10 & 11) records growth zoning as evidenced by the bell-shaped pattern of spessartine (from 3 to 0.1 wt% MnO) and overall decrease in Fe/(Fe + Mg) from core to left rim (0.92–0.89). The inclusion pattern is curved and continuous with the fabric outside the garnet, suggesting syntectonic growth. This garnet has lower grossular and increased pyrope content near its larger quartz inclusions, leading to the irregular zoning pattern from core to right rim seen in Fig. 11. The *P–T* conditions estimated for MCT shear zone rocks CMP860 and CHG14103 (Fig. 6) are similar to those reported by Lal *et al.* (1981) (560–583 °C), Mohan *et al.* (1989) (594–659 °C, 5–8 kbar) and Dubey (1993) (546–575 °C, 5–6 kbar).

Lesser Himalaya samples KBP1062A (610 ± 25 °C; 7.5 ± 0.5 kbar; Fig. 6) and KBP1062C also contain *c.* 12–13 Ma monazite inclusions in garnet, similar those analyzed in MCT shear zone rocks (Table 3). The KBP1062A garnet is large (> 3 mm in diameter) and shows the effects of diffusion or retrograde resorption by the sharp increase in spessartine (from 0.01 to 0.07) and Fe/(Fe + Mg) (from 0.85 to 0.88) at the rim (Fig. 12). Overall, this garnet has smaller quartz and ilmenite inclusions in the core, a larger quartz region at mid-rim, and small ilmenite and monazite inclusions in the outer rim. The outer rim and core inclusions appear to be aligned in different orientations. Grossular content decreases from core to rim (from 0.08 to 0.04) with a relatively steep decline outward of the large quartz inclusions (Fig. 12), suggesting that the garnet may have grown during decompression (Spear, 1993). Mohan *et al.* (1989) reports similar peak conditions for Lesser Himalaya samples (582–635 °C, *c.* 7.6 kbar).

The following observations can be made from north to south through the Greater Himalayan Crystallines, MCT shear zone and Lesser Himalaya: (1) average monazite ages decrease from Miocene (*c.* 22 Ma) to Late Miocene (14–10 Ma) (see Tables 1–3); (2) garnet grossular patterns change from patchy zoning (LCG541, CMP860) to relatively flat (CHG14103) or decreasing from core to rim (KBP1062A); and (3) garnet appears to begin to preserve growth zoning patterns (compare LCG541 & CHG14103).

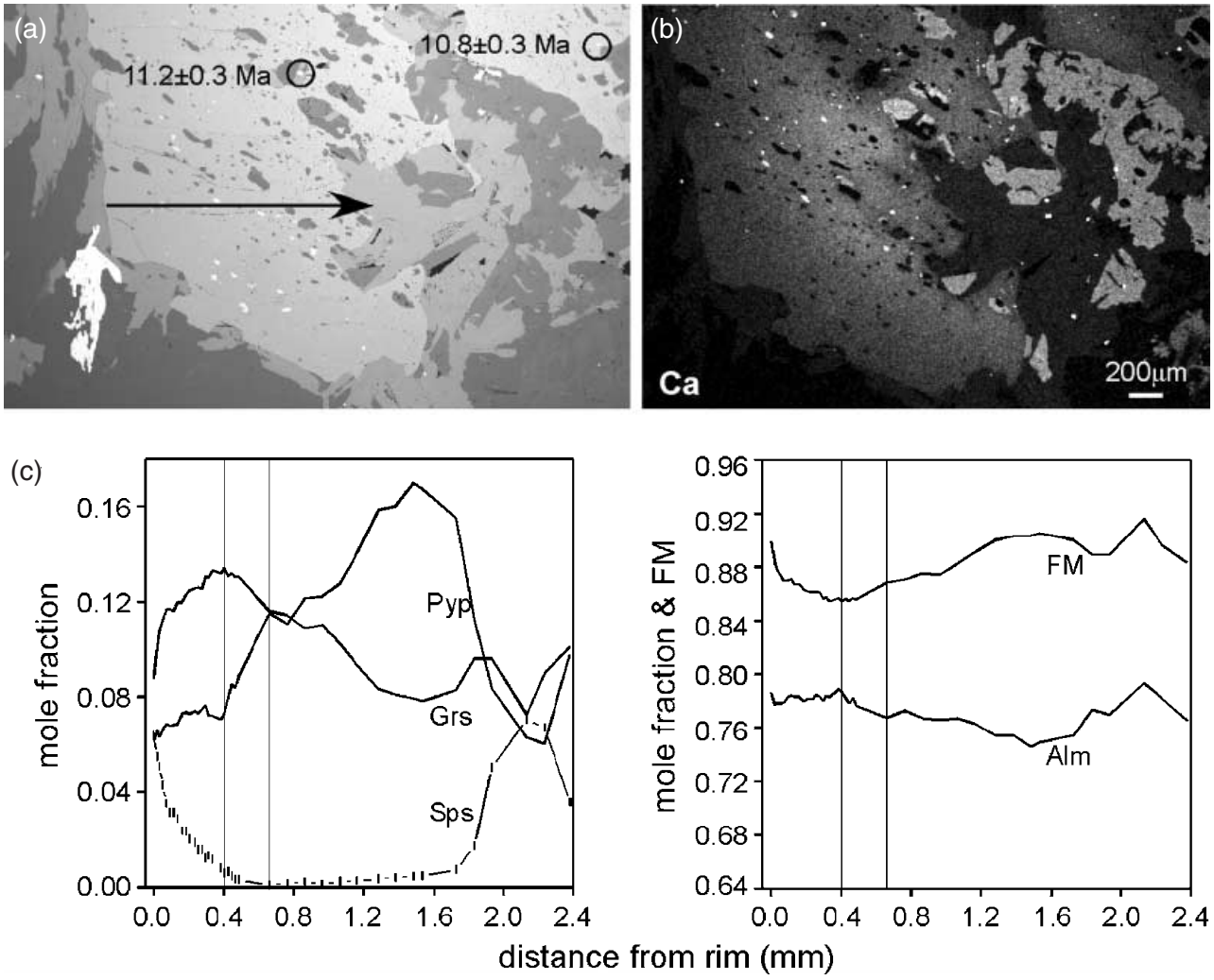

Fig. 9. (a) CMP860 garnet BSE image; (b) Ca X-ray map; and (c) zoning profiles of mole fraction pyrope (Pyp), grossular (Grs), spessartine (Sps), Fe/(Fe + Mg) (FM), and almandine (Alm). Circles in the BSE image encompass dated monazite grains 9 and 10 (see also Fig. 8). See Table 2 for details of the age analyses. The scale for the element map is white = high, black = low Ca concentration. The element map also shows bright white spots, which are small grains of apatite or allanite. The arrow in the BSE image is the approximate path where compositional analyses were taken. Tick marks on the spessartine profile show the position of each analysis; the length of each tick has no statistical significance. The longer vertical lines are positions of compositions used for *P–T* calculations; see Table 5 for numerical values.

We expected thermal conditions to change from high (*c*. 700 °C) to lower temperatures (*c*. 525 °C) moving south through the shear zone, but one Lesser Himalaya sample (KBP1062A) appears to record a higher temperature and potentially higher pressure than the MCT shear zone rock (CHG14103; Fig. 6). The *P–T* conditions estimated for these samples are consistent with their mineral assemblages and previous work by other researchers (e.g. Lal *et al*., 1981; Mohan *et al*., 1989; Dubey, 1993). Further examination of the individual monazite ages in KBP1062A shows that it experienced monazite crystallization coeval with and prior to the structurally lower rock, suggesting that observation (1) may be a simplification of a complicated monazite crystallization history within the MCT shear zone.

TIMING CONSTRAINTS ON STDS SLIP

In northern Sikkim, the STDS (Fig. 1) is present in close proximity to the Pauhunri Granite: a several 100 km^3 leucogranite body comprising coalesced sills and laccoliths that intrude the para- and orthogneiss of the Greater Himalayan Crystallines. Sample MK51K was collected from a slightly deformed horizon of a High Himalayan leucogranite pluton, observed in the field as part of an extensive injection complex.

U–Pb ages of zircon separated from the MK51K leucogranite are rarely concordant (Fig. 13), and range from Paleo-Mesoproterozoic (e.g. grain 9–1, 2512 ± 9 Ma and grain 7–2, 960 ± 35 Ma, $^{207}Pb/^{206}Pb$ ages) to Miocene age (e.g. grain 6–2,

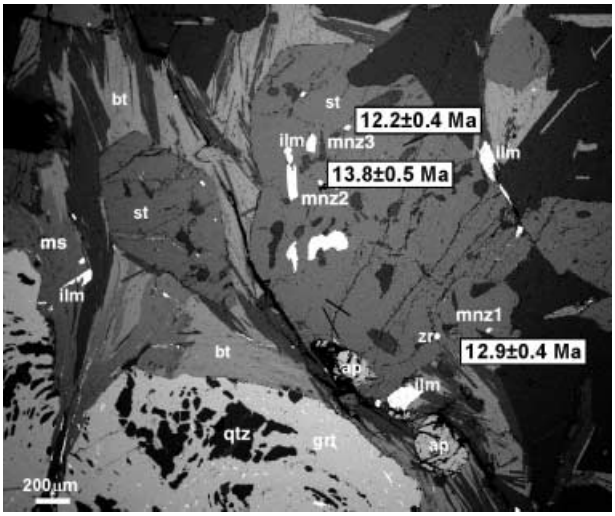

Fig. 10. BSE image of MCT shear zone rock CHG14103. All dated monazite are indicated with grain number (mnz#) and age ($\pm$ 1σ). Other abbreviations include 'grt', garnet, 'bt', biotite, 'qtz', quartz, 'ap', apatite, 'ilm', ilmenite, 'ms', muscovite and 'st', staurolite. See Table 2 for details of the age analyses.

17.2 $\pm$ 0.4 Ma and grain 5–2, 16.2 $\pm$ 0.2 Ma, $^{206}Pb/^{238}U$ age; see Table 8). The age range and zircon concordia plots suggest that the grains have experienced Pb loss. Many analyses may also be affected by inheritance as older ages are generally found within visible cores of the zircon grains, whereas younger ages are found near the rims. For example, spots on the core of zircon 6 are *c*. 500 Ma, whereas the rim is as young as 17.2 $\pm$ 0.4 Ma ($^{206}Pb/^{238}U$ age; Fig. 3). A number of zircon yield Pan African ages (see $^{207}Pb/^{206}Pb$ ages of grains 1, 2, 4, 6 and 8), consistent with numerous Cambro-Ordovician ages reported from the Himalayan belt elsewhere (e.g. Le Fort *et al*., 1986; Valdiya, 1993; Miller *et al*., 2001). Although many zircon yield *c*. 70 to *c*. 300 Ma U–Pb ages, these results may be attributed to Pb loss or overlapping analyses of different age domains within a single grain. Miocene $^{206}Pb/^{238}U$ ages recorded by zircon 5–1, 5–2 and 6–2 are consistent with monazite ages of leucogranites exposed near the STDS in eastern Nepal (Qomolangma detachment: Murphy & Harrison, 1999).

Monazite may form in igneous rocks via reactions with apatite or REE phosphate minerals (Sawka *et al*., 1986; Wolf & London, 1995). Th–Pb ages of monazite grains from MK51K range from 20.9 $\pm$ 1.7 to 14.8 $\pm$ 0.3 Ma (Table 9 & Fig. 4), with the average being 17.0 $\pm$ 0.8 Ma. Although these monazite were separated from a single rock, the results are inconsistent with a single population (mean square weighted deviation = 8.5). The monazite ages may reflect diffusional Pb loss, resetting due to retrograde reactions, analyses of overlapping age domains, or episodic monazite growth (Catlos *et al*., 2002b). The monazite ion microprobe calibration curve has a correlation coefficient of 0.999 (Table 9), thus we conclude that analytic uncertainties are not the cause of the broad age distribution. Recent diffusion studies of synthetic monazite suggest that this degree of Pb loss is not feasible at these conditions, suggesting the ages do not reflect Pb loss (e.g. Cherniak *et al*., 2000, 2003). This observation, coupled with location of the MK51K granite with respect to the STDS, the rim zircon analyses at *c*. 17 Ma, and consistent data collected at similar structural levels in eastern Nepal (e.g. Murphy & Harrison, 1999) and elsewhere (e.g. Schärer, 1984; Noble & Searle, 1995; Harrison *et al*., 1997b), strongly suggests that the monazite ages younger than *c*. 20 Ma represent continued melting, perhaps related to the slip history of the STDS. Statistical analyses of the younger ages indicate that they could be divided into two populations at 17.5 $\pm$ 0.9 Ma (MSWD = 3) and 15.2 $\pm$ 0.4 Ma (MSWD = 0.8). Thus, the MK51K monazite and zircon ages may reveal anatexis of the MCT hangingwall at 20.5 $\pm$ 1.3 Ma (average of grains 15–1 and 20–1) and two episodes of leucogranite generation or STDS slip at *c*. 17 and *c*. 15 Ma.

DISCUSSION AND CONCLUSIONS

Modelling the Sikkim MCT and STDS

Figure 14 outlines a schematic model of the development of the Sikkim Himalayas. The figure was constructed by categorizing the overall results into four major time periods: at *c*. 22–20 Ma (Fig. 14a), *c*. 18–17 Ma (Fig. 14b), *c*. 14–13 Ma (Fig. 14c) and *c*. 11–10 Ma (Fig. 14d). Note that the sample positions depicted in Fig. 14 are based on the *P–T* constraints reported in this paper. For example, CMP860 experienced similar baric conditions to the other MCT shear zone sample CHG14103, but higher temperatures (Fig. 6), probably due to its closer proximity to the hotter hangingwall.

Monazite dated in Greater Himalayan Crystallines and the MCT shear zone suggest that the structure was active during the early Miocene (*c*. 22 Ma). In Fig. 14(a), the average monazite ages of LCG541, LCG542 and NLG963, the average monazite ages of grains 7 and 3 from MCT shear zone rock CMP860 and the average monazite ages of grains 2 and 15 from leucogranite sample MK51K are indicated. It can be reasonably assumed from the close proximity of these samples to the MCT that monazite crystallized in these rocks due to slip along the structure. The *c*. 20 Ma monazite dated from sample MK51K suggests that High Himalayan leucogranite anatexis also began at this time in the rock package currently forming the Sikkim Greater Himalayan Crystallines. Harrison *et al*. (1998) estimated that heating via a shear stress of *c*. 20–30 MPa along the thrust flat that cuts through Indian rocks is sufficient to produce the leucogranite melts.

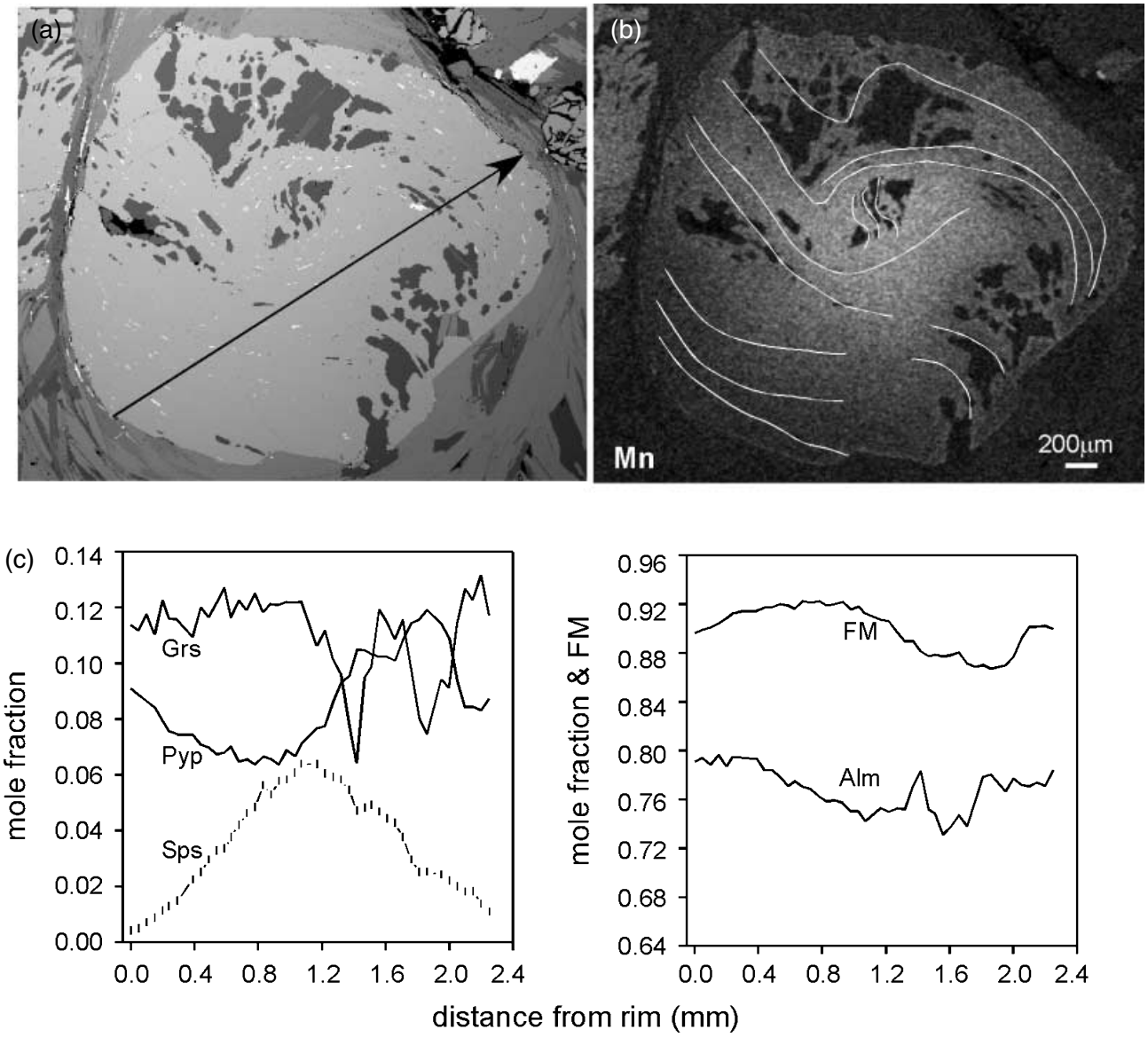

Fig. 11. (a) CHG14103 garnet BSE image; (b) Mn X-ray map; and (c) zoning profiles of mole fraction pyrope (Pyp), grossular (Grs), spessartine (Sps), Fe/(Fe + Mg) (FM), and almandine (Alm). The scale for the element map is white = high, black = low Mn concentration, and white lines follow the ilmenite and quartz inclusion pattern. The arrow in the BSE image is the approximate path where compositional analyses were taken. Tick marks on the spessartine profile show the position of each analysis; the length of each tick has no statistical significance. Spots on the garnet rim had lower Mn and Fe/(Fe + Mg) values than seen in these profiles, thus these compositions were used to estimate the *P–T* conditions (see Table 6).

In Fig. 14(b), the STDS is assumed to initiate at *c*. 17 Ma, based on the 17.5 ± 0.9 Ma average of the monazite age cluster from MK51K, the 16.8 ± 0.3 Ma average age recorded by zircon grains 5 and 6 separated from the same leucogranite, and the structural relationship of the Pauhunri granite to the STDS. The *c*. 17 Ma initiation age of the STDS is similar to monazite ages reported by Murphy & Harrison (1999) for rocks at similar structural levels in eastern Nepal. Tectonic exhumation may have played a role in decompression melting in this area, and we note that this proto-STDS (if indeed present) was likely a more diffuse structure than seen today.

Lesser Himalaya sample KBP1062C has a single 18.3 ± 0.1 Ma matrix monazite. This grain is large (*c*. 65 μm × 45 μm), euhedral, and found as an inclusion in biotite. This age may be the result of: (1) Pb loss from a *c*. 22 Ma grain; (2) a crystallization event related to MCT movement at this time; or (3) a crystallization event not related to MCT movement but facilitated by Miocene emplacement of the Greater Himalayan

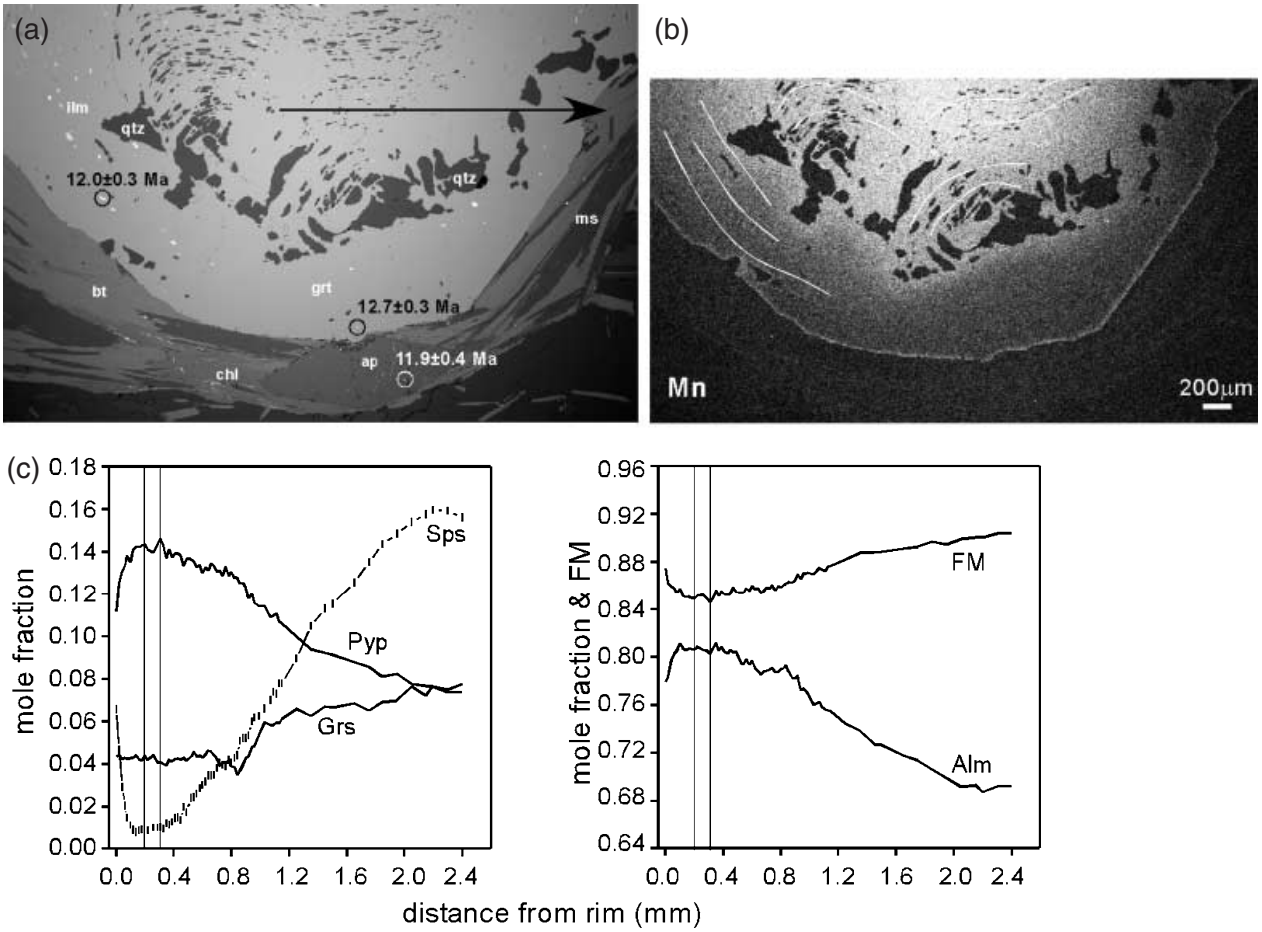

Fig. 12. (a) KBP1062A garnet BSE image; (b) Mn X-ray map; and (c) zoning profiles of mole fraction pyrope (Pyp), grossular (Grs), spessartine (Sps), Fe/(Fe + Mg) (FM), and almandine (Alm). The scale for the element map is white = high, black = low Mn concentration, and white lines follow the ilmenite and quartz inclusion pattern. The arrow in the BSE image is the approximate path where compositional analyses were taken. Circles encompass dated monazite grains 5, 6 and 9 (see Table 3). Tick marks on the spessartine profile show the position of each analysis; the length of each tick has no statistical significance. The longer vertical lines are positions of compositions used for *P–T* calculations; see Table 7 for numerical values. Abbreviations include 'grt', garnet, 'bt', biotite, 'qz', quartz, 'ap', apatite, 'ilm', ilmenite and 'mus', muscovite.

Crystallines. The first suggests that the rock experienced conditions not only conducive to monazite growth during Miocene MCT movement, but also hot enough that the grain experienced *c.* 18% Pb loss. However, garnet crystallized in this rock between 12.2 ± 0.1 and 11.5 ± 0.2 Ma, based on its monazite inclusions (Table 3), thus the question of why garnet would fail to appear at *c.* 18 Ma remains unanswered. The second scenario is that the MCT shear zone at this structural level experienced movement at *c.* 18 Ma; however, MCT slip may not necessarily lead to monazite growth. Another possibility is that heat migrated from the hotter Greater Himalayan Crystallines nappe to the Lesser Himalaya sample at this time, causing the monazite growth in a rock that had a unique bulk composition conducive to the formation of this mineral. The Lesser Himalaya rock was far from the Greater Himalayan Crystallines, thus would experience crystallization *c.* 4 Myr after MCT movement. In any case, these Miocene grains may have provided the source material for subsequent monazite crystallization in KBP1062C.

During the next episode outlined in Fig. 14(c), the STDS continued activity at 15.2 ± 0.4 Ma, whereas the MCT shear zone developed as Lesser Himalaya and MCT shear zone monazite record 14–12 Ma ages. Two matrix monazite grains from CMP860 (14.3 ± 0.7 Ma) and KBP1062A (14.2 ± 1.1 Ma) overlap in age with the youngest MK51K leucogranite monazite age (14.8 ± 0.3 Ma). If these monazite ages record crystallization due to tectonic activity, they are the only geochronological constraints available thus far that clearly identify simultaneous MCT and STDS slip. Overall, monazite ages from the MK51K leucogranite bracket the time period when anatexis occurred within the Greater Himalayan Crystallines from 20.9 ± 1.7 to 14.8 ± 0.3 Ma (Table 8), which provides a striking example of the continual nature of melt production within the orogenic belt.

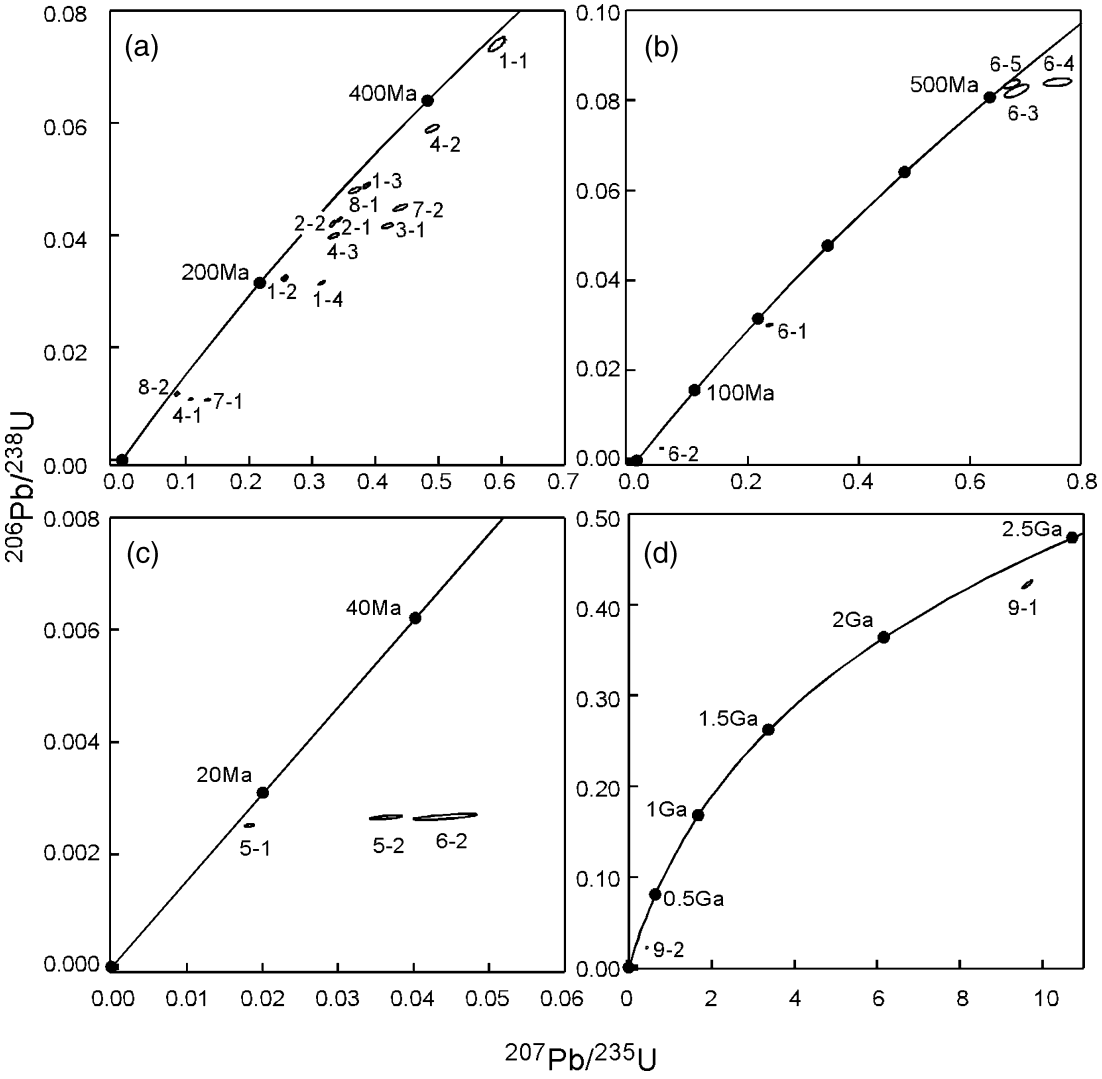

Fig. 13. Concordia plots of MK51K ion microprobe zircon analyses. Each spot analysis is labelled with the grain spot number (see Table 8 and Fig. 3), and concordia is labelled with ages for reference.

In Fig. 14(d), we report the youngest monazite grains dated in each of the MCT footwall rocks in this study. Their ages show that the Sikkim MCT shear zone continued activity at various structural levels at *c*. 10 Ma.

Implications for Himalayan models

Models developed to explain Himalaya petrogenesis are routinely exported as paradigms for similar phenomena in other orogenic belts. For example, inverted metamorphic gradients in the Monashee complex, south-eastern Canadian Cordillera, have been suggested to form via the downward transfer of heat from an overlying nappe (Parrish, 1995) (*à la* Le Fort, 1975) or via synmetamorphic ductile inversion of isograds by progressive shear strain (Gibson *et al*., 1999) (*à la* Hubbard, 1996). Wedge extrusion (*à la* Hodges *et al*., 1993) has been also been applied to the same area (Johnston *et al*., 2000). Extension associated with thickened continental lithosphere (*à la* Dewey, 1988) has even been explored as a possibility to create tessera terrain on Venus (Gilmore *et al*., 1998).

The evolutionary model for Himalayan development as outlined by Seeber & Gornitz (1983) is based on traditional rules for thrust geometry in thin-skinned terrains. The age data reported here document a structural sequence more complicated than generic models of thrust propagation. At the time of thrust initiation, contractional deformation progresses at the regional scale towards the foreland, but the hinterland of orogenic belts may continue to thicken internally (e.g. Burbank *et al*., 1992; Attoh *et al*., 1997; Gray & Mitra, 1999). In this scenario, erosion and accretion of frontal imbricate thrust sheets decrease the thrust-belt

Table 8. U–Pb ages of Sikkim zircon, sample MK51K.[a]

Grain-spot[b]	$^{206}Pb/238U$ age (Ma) ($\pm$ σ)	$^{207}Pb/^{235}U$ age (Ma) ($\pm$ σ)	$^{207}Pb/^{206}Pb$ age (Ma) ($\pm$ σ)	UO^+/U^+ ($\pm$ σ)
9–1	2272 (19)	2401 (11)	2512 (9)	11.28 (0.08)
6–4	520 (5)	573 (14)	789 (64)	11.81 (0.09)
6–5	518 (6)	524 (9)	552 (37)	11.58 (0.05)
6–3	509 (9)	529 (13)	620 (48)	11.53 (0.14)
1–1	460 (4)	472 (5)	528 (19)	11.55 (0.04)
4–2	369 (4)	402 (7)	593 (34)	11.39 (0.06)
1–3	308 (3)	332 (4)	504 (20)	11.42 (0.06)
8–1	299 (4)	319 (7)	465 (41)	11.23 (0.05)
7–2	283 (4)	371 (8)	960 (35)	11.35 (0.05)
2–1	271 (2)	300 (3)	537 (14)	11.53 (0.04)
2–2	266 (3)	292 (3)	509 (20)	11.75 (0.08)
3–1	265 (3)	356 (6)	1006 (35)	11.09 (0.06)
4–3	252 (3)	291 (6)	620 (38)	11.88 (0.08)
1–2	206 (2)	232 (3)	505 (20)	11.69 (0.04)
1–4	200 (2)	278 (4)	998 (17)	11.28 (0.05)
6–1	191 (2)	217 (4)	512 (37)	11.48 (0.04)
9–2	139 (2)	369 (5)	2298 (12)	11.49 (0.08)
8–2	69.5 (0.9)	85.2 (2.0)	552 (33)	11.56 (0.03)
4–1	68.8 (1.0)	104 (3)	1021 (49)	11.45 (0.04)
7–1	68.4 (0.9)	129 (3)	1471 (44)	11.26 (0.06)
6–2	17.2 (0.4)	43.9 (4.1)	1955 (144)	11.50 (0.06)
5–1	17.1 (0.2)	36.2 (2.1)	1604 (96)	11.63 (0.02)
5–2	16.2 (0.2)	18.4 (0.6)	314 (70)	11.69 (0.05)
MK51K zircon calibration: $(1.249 \pm 0.021)x + (0.586 \pm 0.120)$; $r^2 = 0.896$; $UO^+/U^+ = 8.720 \pm 3.186$[d]				

[a] The nomenclature is the grain number-analysis spot number. Note that the table is arranged by descending $^{206}Pb/^{238}U$ age. See Fig. 3 for transmitted light images and Fig. 13 for concordia plots of these dated zircon.
[b] Measured ratio in sample.
[c] Zircon calibration information: sample name, best fit of the calibration to the equation of a line (slope*x + intercept) with $\pm$ 1σ uncertainty, correlation (r^2), and range of UO^+/U^+ ($\pm$ 1σ) measured using zircon standard AS3 (e.g. Schneider *et al.*, 1999). Ideally, the unknown UO^+/U^+ lies within the UO^+/U^+ range defined by the standard.

Table 9. Th–Pb ages of Sikkim monazite, sample MK51K.

Grain–spot[a]	Age (Ma) ($\pm$ σ)	ThO_2^+/Th^+[b] ($\pm$ σ)	^{208}Pb (%)[c] ($\pm$ σ)	$^{208}Pb^*/Th^+$[d] ($\pm$ σ)
2–1	20.9 (1.7)	5.577 (0.009)	96.6 (0.3)	1.033E−03 (8.440E−05)
15–1	20.1 (0.7)	6.390 (0.016)	97.1 (0.3)	9.971E−04 (3.294E−05)
8–1	18.1 (1.1)	5.901 (0.013)	98.1 (0.2)	8.980E−04 (5.294E−05)
4–1	18.1 (1.2)	5.827 (0.010)	96.9 (0.3)	8.977E−04 (5.724E−05)
4–3	17.9 (1.1)	5.840 (0.006)	97.0 (0.3)	8.855E−04 (5.565E−05)
4–2	17.5 (1.0)	5.955 (0.015)	96.8 (0.3)	8.663E−04 (4.846E−05)
1–2	17.4 (0.5)	6.443 (0.017)	94.0 (0.6)	8.597E−04 (2.594E−05)
13–1	16.8 (0.6)	6.327 (0.006)	95.4 (0.4)	8.321E−04 (2.953E−05)
14–1	16.7 (0.2)	6.967 (0.018)	96.2 (0.5)	8.285E−04 (1.012E−05)
1–1	15.5 (0.4)	6.468 (0.013)	95.5 (0.5)	7.687E−04 (2.225E−05)
1–3	15.6 (0.5)	6.471 (0.012)	91.2 (0.7)	7.737E−04 (2.335E−05)
7–1	15.4 (0.6)	6.268 (0.015)	81.6 (0.9)	7.595E−04 (3.058E−05)
3–1	15.0 (0.4)	6.473 (0.014)	96.6 (0.4)	7.420E−04 (2.117E−05)
5–1	14.8 (0.3)	6.696 (0.011)	95.7 (0.4)	7.334E−04 (1.463E−05)
6–1	14.8 (0.3)	6.633 (0.017)	95.1 (0.5)	7.306E−04 (1.637E−05)
MK51K monazite calibration: $(0.097 \pm 0.014)x + (2.653 \pm 0.671)$; $r^2 = 0.999$; $ThO2^+/Th^+ = 7.248 \pm 0.246$[e]				

[a] The nomenclature is the grain number-analysis spot number. Note that the table is arranged by descending Th–Pb age. See Fig. 5 for transmitted light images of these dated grains. Note that the average age is 17.0 $\pm$ 0.8 Ma, MSWD = 8.5.
[b] Measured ratio in sample.
[c] Percentage radiogenically derived ^{208}Pb.
[d] Corrected sample ratio assuming $^{208}Pb/^{204}Pb = 39.5 \pm 0.1$ (Stacey & Kramers, 1975).
[e] Calibration information: sample name, best fit of the calibration to the equation of a line (slope*x + intercept) with $\pm$ 1σ uncertainty, correlation (r^2), and range of ThO_2^+/Th^+ ($\pm$ 1σ) measured using monazite 554 (e.g. Harrison *et al.*, 1999b). Ideally, the unknown ThO_2^+/Th^+ lies within the ThO_2^+/Th^+ range defined by the standard.

taper, which in turn drives internal deformation. The evidence suggests that synchronous thrusting and out-of-sequence imbrication are mechanisms in which the Himalayan wedge maintains a critical taper (e.g. Davis *et al.*, 1983; Seeber & Gornitz, 1983; Boyer, 1992). The feasibility of out-of-sequence thrusting as a mechanism for accommodating convergence is further supported by the documentation of large-scale out-of-sequence events in other contractional terrains (see Gessner *et al.*, 2001).

The Late Miocene ages of Sikkim monazite grains are wholly consistent with a MCT shear zone that was active at the same time as that documented by the MBT elsewhere (e.g. Meigs *et al.*, 1995; Upreti, 1999). In this way, the Himalayan range does not solely follow a sequence of deformation in which convergence shifts towards the foreland as mountain building progressed, but instead records out-of-sequence thrusting. Pressure conditions recorded by the garnet rim in sample CMP860 (6 $\pm$ 1 kbar), the precise age of the monazite inclusion (10.8 $\pm$ 0.3 Ma), and a lithostatic gradient suggest that the exhumation rate of the MCT shear zone in the Sikkim region is estimated to be *c.* 2 mm yr^{-1} [= 6 kbar/(0.27 kbar km^{-1} × 10.8 Ma)], similar to that calculated for eastern Nepal (Catlos *et al.*, 2002a).

Individual monazite ages from the MCT shear zone fail to show a progressive younging distribution, and thus are inconsistent with the hypothesis that the region can be modelled as a duplex, in which successive MCT footwall slivers are excised and incorporated into the hangingwall (Robinson *et al.*, 2003). Although the presence of *c.* 15–14 Ma monazite grains in both the MCT shear zone and STDS-deformed High Himalayan leucogranite supports the idea that the structures may have operated simultaneously at this time, further geochronological constraints suggest that the picture is more complicated than pure wedge extrusion or pure channel flow. The two structures appear to converge at the Main Himalayan Thrust at depth (Nelson *et al.*, 1996), indicating that they are linked by their structural geometry, but their temporally distinct monazite ages at *c.* 17 and *c.* 12–10 Ma suggest that the structures operated independently at these times, lending support to an orogenic-collapse-type scenario. In Sikkim, the MCT was active at 22–20, 15–14 and 12–10 Ma, whereas the STDS may have been active at *c.* 17 and 15–14 Ma.

The *in situ* monazite ages from the Sikkim region are similar to *c.* 14 Ma monazite ages found in several rocks collected *c.* 150 km west along the Dudh Kosi–Everest transect in eastern Nepal (Catlos *et al.*, 2002a). For example, the CMP860 inclusion age of 10.8 $\pm$ 0.3 Ma is within error of a 10.3 $\pm$ 0.8 Ma monazite inclusion in garnet found at similar structural levels in eastern Nepal. The *c.* 17 Ma timing constraint from MK51K is similar to monazite ages of leucogranites exposed near the STDS in eastern Nepal (Murphy & Harrison, 1999). These geochronological results indicate the lateral continuity of orogenic events in eastern Nepal and NE India.

The thermobarometric conditions and presence of 14–10 Ma monazite inclusions in garnet from rocks

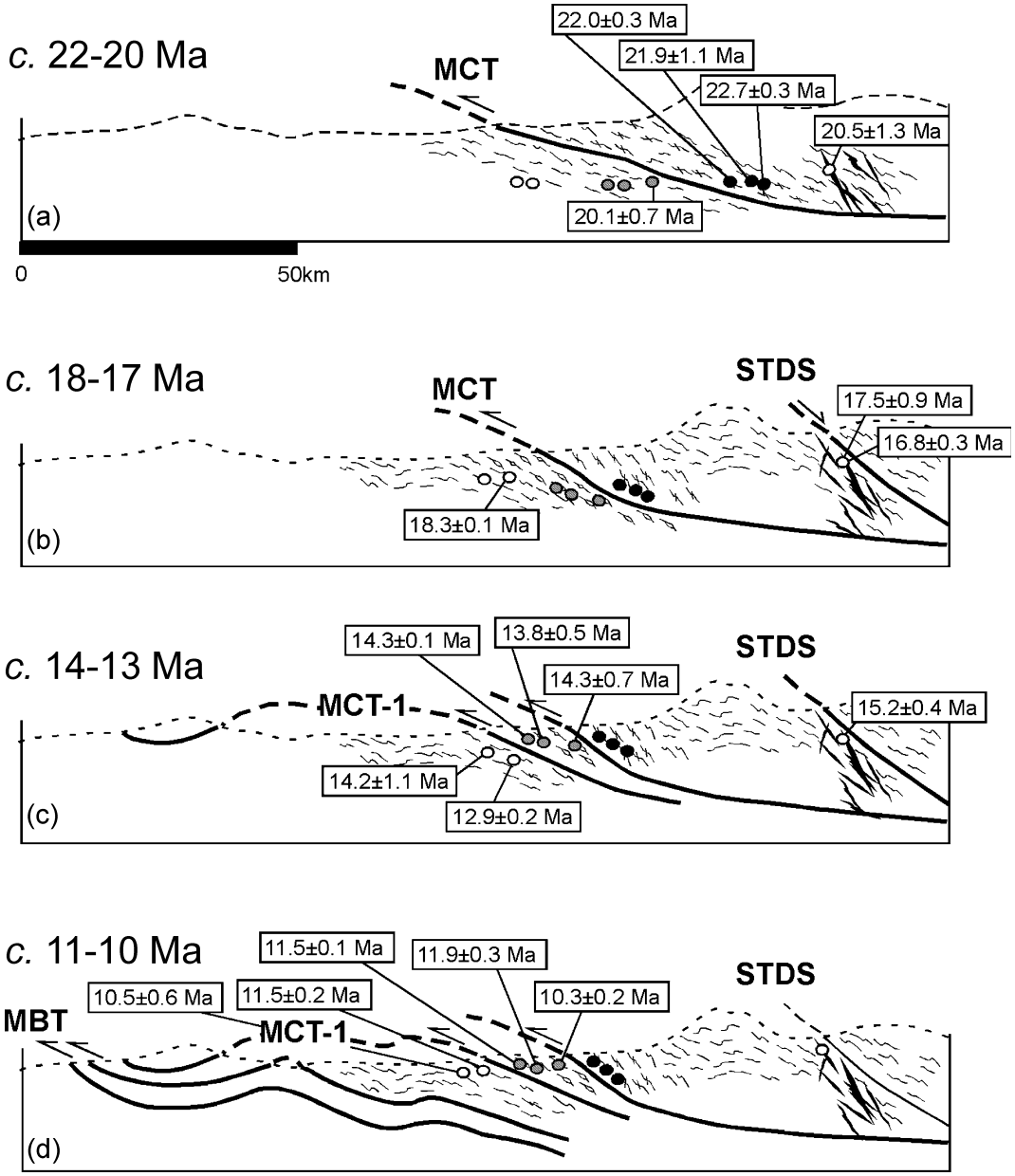

Fig. 14. Schematic interpretation of the age results and *P–T* constraints from Sikkim rocks. See the text for the full explanation. Note that the Greater Himalayan Crystallines rocks (samples NLG963, LCG542 and LCG541) are indicated by black circles, whereas the MCT shear zone samples (CMP860, CHG14104 and CHG14103) are grey and the Lesser Himalaya samples (KBP1062A and KBP1062C) are white. The High Himalayan leucogranite MK51K is indicated in white as well.

collected from the inverted sequence suggest that specific thrusts were active within the shear zone, creating the apparent inverted metamorphism observed in the field (e.g. Harrison *et al.*, 1997a, 1998). Although rocks collected from the Sikkim region did not record Pliocene monazite ages as seen in central Nepal (Catlos *et al.*, 2001), the nappe structures in this area may obscure the reactivated ramp, or our samples may lie outside areas that experienced younger slip. Mukul (2000) indicates that the region between the MCT and MBT is the locus of 4.5–6.8 (Mb) magnitude earthquakes since 1960–98, leaving open the possibility that the Sikkim MCT shear zone is presently active.

ACKNOWLEDGEMENTS

We acknowledge support from the Instrumentation and Facilities Program of the National Science Foundation. Ion microprobe analyses were conducted at the National Ion Microprobe Facility at UCLA, whereas the CAMECA Camebax at UCLA was used to obtain the electron microprobe analyses. We thank

Dr A. Meigs and Dr M. Williams for constructive and detailed reviews.

REFERENCES

Attoh, K., Dallmeyer, R. D. & Affaton, P., 1997. Chronology of nappe assembly in the Pan-African Dahomeyide orogen, West Africa: Evidence from $^{40}Ar/^{39}Ar$ mineral ages. *Precambrian Research*, **82,** 153–171.

Ayers, J. C., Miller, C., Gorisch, B. & Milleman, J., 1999. Textural development of monazite during high-grade metamorphism: Hydrothermal growth kinetics, with implications for U,Th–Pb geochronology. *American Mineralogist*, **84,** 1766–1780.

Berman, R. G., 1990. Mixing properties of Ca–Mg–Fe–Mn garnets. *American Mineralogist*, **75,** 328–344.

Bordet, P., Colchen, M. & Le Fort, P., 1975. *Recherches Géologiques Dans l'Himalaya Du Népal, Région Du Nyi-Shang*, p. 1–138. Centre National de la Recherches Scientifiques, Paris.

Boyer, S. E., 1992. Geometric evidence from synchronous thrusting in the southern Alberta and northwest Montana thrust belts. In: *Thrust Tectonics* (ed. McClay, K. R.), pp. 377–390. Chapman & Hall, London.

Burbank, D. W., Verges, J., Mufioz, J. A. & Bentham, P., 1992. Coeval hindward and forward-imbricating thrusting in the south central Pyrenees, Spain: Timing and rates of shortening and deposition. *Geological Society of America Bulletin*, **104,** 3–17.

Catlos, E. J., Gilley, L. D. & Harrison, T. M., 2002b. Interpretation of monazite ages obtained via in situ analysis. *Chemical Geology*, **188,** 193–215.

Catlos, E. J., Harrison, T. M., Kohn, M. J., Grove, M., Ryerson, F. J., Manning, C. E. & Upreti, B. N., 2001. Geochronologic and thermobarometric constraints on the evolution of the Main Central Thrust, central Nepal Himalaya. *Journal of Geophysical Research*, **106,** 16177–16204.

Catlos, E. J., Harrison, T. M., Manning, C. E. *et al.*, 2002a. Records of the evolution of the Himalayan orogen from in situ Th–Pb ion microprobe dating of monazite: Eastern Nepal and Garhwal. *Journal of Asian Earth Sciences*, **20,** 459–479.

Cherniak, D. J. & Watson, E. B., 2001. Pb diffusion in zircon. *Chemical Geology*, **172,** 5–24.

Cherniak, D. J., Watson, E. B., Grove, M. & Harrison, T. M., 2003. Pb diffusion in monazite: a combined RBS/SIMS study. *Geochimica et Cosmochimica Acta*, **68,** 829–840.

Cherniak, D. J., Watson, E. B., Harrison, T. M. & Grove, M., 2000. Pb diffusion in monazite: a progress report on a combined RBS/SIMS study. *American Geophysical Union, EOS Transactions*, **81,** S25.

Cressey, G., Wall, F. & Cressey, B. A., 1999. Differential REE uptake by sector growth of monazite. *Mineralogical Magazine*, **63,** 813–828.

Davidson, C., Grujic, D. E., Hollister, L. S. & Schmid, S. M., 1997. Metamorphic reactions related to decompression and synkinematic intrusion of leucogranite, High Himalayan Crystallines, Bhutan. *Journal of Metamorphic Geology*, **15,** 593–612.

Davis, D., Suppe, J. & Dahlen, F. A., 1983. Mechanics of fold-and-thrust belts and accretionary wedges. *Journal of Geophysical Research*, **88,** 1153–1172.

Dewey, J. F., 1988. Extensional collapse of orogens. *Tectonics*, **7,** 1123–1139.

Dubey, C. S., 1993. Study of the Lesser Himalayan metamorphics, Eastern Sikkim, India, pp. 1–152. *PhD Thesis*, *University of Delhi, India*.

Duncan, C., Masek, J. & Fielding, E., 2003. How steep are the Himalaya? Characteristics and implications of along-strike topographic variations. *Geology*, **31,** 75–78.

Edwards, M. A., Catlos, E. J., Harrison, T. M. & Dubey, C. S., 2002. We seek him now, we sought him then: 70 years of constraints on the STDS in Sikkim. 17th Himalaya–Karakoram–Tibet Workshop, Sikkim, India. *Journal of Asian Earth Sciences*, **20** (Suppl. 1)**,** 11–12.

England, P., Le Fort, P., Molnar, P. & Pêcher, A., 1992. Heat sources for Tertiary metamorphism and anatexis in the Annapurna–Manaslu region, central Nepal. *Journal of Geophysical Research*, **97,** 2107–2128.

Ferry, J. M. & Spear, F. S., 1978. Experimental calibration of partitioning of Fe and Mg between biotite and garnet. *Contributions to Mineralogy and Petrology*, **66,** 113–117.

Florence, F. P. & Spear, F. S., 1991. Effects of diffusional modification of garnet growth zoning on P–T path calculations. *Contributions to Mineralogy and Petrology*, **107,** 487–500.

Fuchs, G., Regmi, K. & Schill, E., 1999. Note on the geology of the Nar-Manang Region in northern Nepal (Himalaya). 14th Himalaya–Karakoram–Tibet Workshop, Kloster Ettal, Germany. *Terra Nostra*, **99,** 46–47.

Fuchs, G., Widder, R. W. & Tuladhar, R., 1988. Contributions to the geology of the Annapurna Range (Manang Area, Nepal). *Jahrbuch der Geologischen Bundesanstalt Wien*, **131,** 593–607.

Ganguly, J., Dasgupta, S., Cheng, W. & Neogi, S., 2000. Exhumation history of a section of the Sikkim Himalayas India: records in the metamorphic mineral equilibria and compositional zoning of garnet. *Earth and Planetary Science Letters*, **183,** 471–486.

Gessner, K., Ring, U., Passchier, C. W. & Gungor, T., 2001. How to resist subduction: Evidence for large-scale out-of-sequence thrusting during Eocene collision in western Turkey. *Journal of the Geological Society of London*, **158,** 769–784.

Gibson, H. D., Brown, R. L. & Parrish, R. R., 1999. Deformation-induced inverted metamorphic field gradients: An example from the southeastern Canadian Cordillera. *Journal of Structural Geology*, **21,** 751–767.

Gilmore, M. S., Collins, G. C. & Ivanov, M. A., 1998. Style and sequence of extensional structures in tessera terrain, Venus. *Journal of Geophysical Research*, **103,** 16813–16840.

Gray, M. B. & Mitra, G., 1999. Ramifications of four-dimensional progressive deformation in contractional mountain belts. *Journal of Structural Geology*, **21,** 1151–1160.

Harris, N., Inger, S. & Massey, J., 1993. The role of fluids in the formation of High Himalayan leucogranites. In: *Himalayan Tectonics, 74* (eds Trealor, P. J. & Searle, M. P.), pp. 391–400. Geological Society, London.

Harrison, T. M., Catlos, E. J. & Montel, J.-M., 2002. U–Th–Pb Dating of Phosphate Minerals. In: *Phosphates: Geochemical, Geobiological and Materials Importance* (eds Hughes, J. M., Kohn, M. & Rakovan, J.), pp. 523–558. Mineralogical Society of America, Washington DC.

Harrison, T. M., Grove, M. & Lovera, O. M., 1997b. New insights into the origin of two contrasting Himalayan granite belts. *Geology*, **25,** 899–902.

Harrison, T. M., Grove, M., Lovera, O. M. & Catlos, E. J., 1998. A model for the origin of Himalayan anatexis and inverted metamorphism. *Journal of Geophysical Research*, **103,** 27017–27032.

Harrison, T. M., Grove, M., Lovera, O. M., Catlos, E. J. & D'Andrea, J., 1999a. The origin of Himalayan anatexis and inverted metamorphism: Models and constraints. *Journal of Asian Earth Sciences*, **17,** 755–772.

Harrison, T. M., Grove, M., McKeegan, K. D., Coath, C. D., Lovera, O. M. & Le Fort, P., 1999b. Origin and emplacement of the Manaslu intrusive complex, Central Himalaya. *Journal of Petrology*, **40,** 3–19.

Harrison, T. M., McKeegan, K. D. & Le Fort, P., 1995. Detection of inherited monazite in the Manaslu leucogranite by $^{208}Pb/^{232}Th$ ion microprobe dating: Crystallization age and tectonic implications. *Earth and Planetary Science Letters*, **133,** 271–282.

Harrison, T. M., Ryerson, F. J., Le Fort, P., Yin, A., Lovera, O. M. & Catlos, E. J., 1997a. A Late Miocene–Pliocene origin for central Himalayan inverted metamorphism. *Earth and Planetary Science Letters*, **146,** E1–E8.

Hodges, K. V., 2000. Tectonics of the Himalaya and southern Tibet from two perspectives. *Geological Society of America Bulletin*, **112,** 324–350.

Hodges, K. V., Burchfiel, B. C., Royden, L. H., Chen, Z. & Liu, Y., 1993. The metamorphic signature of contemporaneous extension and shortening in the central Himalayan orogen: Data from the Nyalam transect, southern Tibet. *Journal of Metamorphic Geology*, **11,** 721–737.

Hodges, K. V., Parrish, R. R. & Searle, M. P., 1996. Tectonic evolution of the central Annapurna Range, Nepalese Himalayas. *Tectonics*, **15,** 1264–1291.

Hoisch, T. D., 1990. Empirical calibration of six geobarometers for the mineral assemblage quartz + muscovite + biotite + plagioclase + garnet. *Contributions to Mineralogy and Petrology*, **104,** 225–234.

Hubbard, M. S., 1996. Ductile shear as a cause of inverted metamorphism: example from the Nepal Himalaya. *Journal of Geology*, **104,** 493–499.

Johnston, D. H., Williams, P. F., Brown, R. L., Crowley, J. L. & Carr, S. D., 2000. Northeastward extrusion and extensional exhumation of crystalline rocks of the Monashee complex, southeastern Canadian Cordillera. *Journal of Structural Geology*, **22,** 603–625.

Kohn, M. J. & Spear, F. S., 2001. Retrograde net transfer reaction (ReNTR) insurance for P–T estimates. *Geology*, **28,** 1127–1130.

Lal, R. K., Mukerji, S. & Ackermand, D., 1981. Deformation and Barrovian metamorphism at Takdah, Darjeeling (Eastern Himalaya). In: *Metamorphic Tectonites of the Himalaya* (ed. Saklani, P. S.), pp. 231–287. Today & Tomorrow's Printers and Publishers, New Delhi.

Le Fort, P., 1975. Himalaya, the collided range, Present knowledge of the continental arc. *American Journal of Science*, **275A,** 1–44.

Le Fort, P., 1996. Evolution of the Himalaya. In: *The Tectonic Evolution of Asia* (eds Yin, A. & Harrison, T. M.), pp. 95–109. Cambridge University Press, Cambridge.

Le Fort, P., Debon, F., Pêcher, A. & Sonet, A. V. P., 1986. The 500 Ma magmatic event in alpine southern Asia, a thermal episode at Gondwana scale. In: *Évolution Des Domains Orogéniques d'Asie Méridionale (de la Turquie A l'Indoneasie), 47* (eds Le Fort, P., Colchen, M. & Montenat, C.), pp. 191–209. Science de la Terre, Paris, France.

Meigs, A. J., Burbank, D. W. & Beck, R. A., 1995. Middle-late Miocene (> 10 Ma) formation of the Main Boundary Thrust in the Western Himalaya. *Geology*, **23,** 423–426.

Meldrum, A., Boatner, L. A., Weber, W. J. & Ewing, R. C., 1998. Radiation damage in zircon and monazite. *Geochimica et Cosmochimica Acta*, **62,** 2509–2520.

Miller, C., Thöni, M., Frank, W. *et al.*, 2001. The early Palaeozoic magmatic event in the Northwest Himalaya, India: Source, tectonic setting and age of emplacement. *Geological Magazine*, **138,** 237–251.

Mohan, A., Windley, B. F. & Searle, M. P., 1989. Geothermobarometry and development of inverted metamorphism in the Darjeeling–Sikkim region of the eastern Himalaya. *Journal of Metamorphic Geology*, **7,** 95–110.

Mojzsis, S. J. & Harrison, T. M., 2002. Establishment of a 3.83-Ga magmatic age for the Akilia tonalite (southern West Greenland). *Earth and Planetary Science Letters*, **202,** 563–576.

Montel, J., Kornprobst, J. & Vielzeuf, D., 2000. Preservation of old U–Th–Pb ages in shielded monazite: Example from Beni Bousera Hercynian kinzigites (Morocco). *Journal of Metamorphic Geology*, **18,** 335–342.

Mukul, M., 2000. The geometry and kinematics of the Main Boundary Thrust and related neotectonics in the Darjiling Himalayan fold-and-thrust belt, West Bengal, India. *Journal of Structural Geology*, **22,** 1261–1283.

Murphy, M. A. & Harrison, T. M., 1999. Relationship between leucogranites and the Qomolangma detachment in the Rongbuk valley, south Tibet. *Geology*, **27,** 831–834.

Nelson, K. D., Zhao, W., Brown, L. D. & Project INDEPTH, 1996. Partially molten crust beneath Southern Tibet: Synthesis of project INDEPTH results. *Science*, **274,** 1684–1688.

Neogi, S., Dasgupta, S. & Fukuoka, M., 1998. High P–T polymetamorphism, dehydration melting, and generation of migmatites and granites in the Higher Himalayan crystalline complex, Sikkim, India. *Journal of Petrology*, **39,** 61–99.

Ni, J. & Barazangi, M., 1984. Seismotectonics of the Himalayan collision zone; geometry of the underthrusting Indian Plate beneath the Himalaya. *Journal of Geophysical Research*, **89,** 1147–1163.

Noble, S. R. & Searle, M. P., 1995. Age of crustal melting and leucogranite formation from U–Pb zircon and monazite dating in the western Himalaya, Zanskar, India. *Geology*, **23,** 1135–1138.

Parrish, R. R., 1995. Thermal evolution of the southeastern Canadian Cordillera. *Canadian Journal of Earth Science*, **32,** 1618–1642.

Passchier, C. W. & Trouw, R. A. J., 1996. *Microtectonics*. Springer-Verlag, New York.

Pyle, J. M., Spear, F. S., Rudnick, R. L. & McDonough, W. F., 2001. Monazite–xenotime–garnet equilibrium in metapelites and a new monazite–garnet thermometer. *Journal of Petrology*, **42,** 2083–2107.

Ray, S., 1947. Zonal metamorphism in the eastern Himalayas and some aspects of local geology. *Quarterly Journal of the Geological, Mining and Metallurgical Society of India*, **19,** 117–140.

Robinson, D. M., DeCelles, P. G., Garizone, C. N., Pearson, O. N., Harrison, T. M. & Catlos, E. J., 2003. Kinematic model for the Main Central Thrust in Nepal. *Geology*, **31,** 359–362.

Sawka, W. N., Banfield, J. F. & Chappell, B. W., 1986. A weathering-related origin of widespread monazite in S-type granites. *Geochimica et Cosmochimica Acta*, **50,** 171–175.

Schärer, U., 1984. The effect of initial ^{230}Th disequilibrium on young U–Pb ages: The Makalu case, Himalaya. *Earth and Planetary Science Letters*, **67,** 191–204.

Schneider, D. A., Edwards, M. A., Kidd, W. S. F., Zeitler, P. K. & Coath, C. D., 1999. Early Miocene anatexis identified in the western syntaxis, Pakistan Himalaya. *Earth and Planetary Science Letters*, **167,** 121–129.

Seeber, L. & Gornitz, V., 1983. River profiles along the Himalayan arc as indicators of active tectonics. *Tectonophysics*, **92,** 335–367.

Smith, H. A. & Barreiro, B., 1990. Monazite U–Pb dating of staurolite grade metamorphism in pelitic schists. *Contributions to Mineralogy and Petrology*, **105,** 602–615.

Spear, F. S., 1993. Metamorphic phase equilibria and pressure–temperature–time paths. *Mineralogical Society of America Monograph*, **1,** 511–545.

Stacey, J. S. & Kramers, J. D., 1975. Approximation of terrestrial lead isotope evolution by a two-stage model. *Earth and Planetary Science Letters*, **26,** 207–221.

Stephenson, B. J., Searle, M. P., Waters, D. J. & Rex, D. C., 2001. Structure of the Main Central Thrust zone and extrusion of the High Himalayan deep crustal wedge, Kishtwar–Zanskar Himalaya. *Journal of the Geological Society*, **158,** 637–652.

Townsend, K. J., Miller, C. F., D'Andrea, J. L., Ayers, J. C., Harrison, T. M. & Coath, C. D., 2000. Low temperature replacement of monazite in the Ireteba granite, Southern Nevada: Geochronological implications. *Chemical Geology*, **172,** 95–112.

Upreti, B. N., 1999. An overview of the stratigraphy and tectonics of the Nepal Himalaya. *Journal of Asian Earth Sciences*, **17,** 741–753.

Valdiya, K. S., 1993. Evidence for Pan-African-Cadomian tectonic upheavals in the Himalaya. *Journal of the Palaeontological Society of India*, **38,** 51–62.

Vannay, J.-C. & Hodges, K. V., 1996. Tectonometamorphic evolution of the Himalayan metamorphic core between Annapurna and Dhaulagiri, central Nepal. *Journal of Metamorphic Geology*, **14,** 635–656.

Wing, B. A., Ferry, J. M. & Harrison, T. M., 2003. Prograde destruction and formation of monazite and allanite during contact and regional metamorphism of pelites; petrology and geochronology. *Contributions to Mineralogy and Petrology*, **145,** 228–250.

Wolf, M. B. & London, D., 1995. Incongruent dissolution of REE- and Sr-rich apatite in peraluminous granitic liquids: Differential apatite, monazite, and xenotime solubilities during anatexis. *American Mineralogist*, **80,** 765–775.

Yeats, R. S., Nakata, T., Farah, A. *et al.*, 1992. The Himalayan Frontal Fault System. *Annales Tectonicae*, **6** (Suppl.), 85–98.

Yin, A. & Harrison, T. M., 2000. Geologic evolution of the Himalayan–Tibet orogen. *Annual Reviews in Earth and Planetary Science*, **28,** 211–280.

Zhu, X. K. & O'Nions, R. K., 1999. Zonation of monazite in metamorphic rocks and its implications for high temperature thermochronology: a case study from the Lewisian Terrane. *Earth and Planetary Science Letters*, **171,** 209–220.

Received 24 June 2003; revision accepted 5 January 2004.